1

Introduction

1.1 Photothermal Spectroscopy

Photothermal spectroscopy is a group of high sensitivity methods used to measure optical absorption and thermal characteristics of a sample. The basis of photothermal spectroscopy is a *photo*induced change in the *thermal* state of the sample. Light energy absorbed and not lost by subsequent emission results in sample heating. This heating results in a temperature change as well as changes in thermodynamic parameters of the sample that are related to temperature. Measurements of the temperature, pressure, or density changes that occur due to optical absorption are ultimately the basis for the photothermal spectroscopic methods.

Ingle and Crouch (1988) classify photothermal spectroscopy as one of several indirect methods for optical absorption analysis. Indirect methods do not measure the transmission of light used to excite the sample directly, but rather measure an effect that optical absorption has on the sample. The term indirect applies to the light measurement, not to the optical absorbance. Photothermal spectroscopy is, in a sense, a more direct measure of optical absorption than optical transmission-based spectroscopies. Sample heating is a direct consequence of optical absorption, and so photothermal spectroscopy signals are directly dependent on light absorption. Scattering and reflection losses do not produce photothermal signals. Subsequently, photothermal spectroscopy more accurately measures optical absorption in scattering solutions, in solids, and at interfaces. This aspect makes it particularly attractive for application to surface and solid absorption studies and studies in scattering media.

The indirect nature of the measurement also results in photothermal spectroscopy being more sensitive than optical absorption measured by transmission methods. There are two reasons for this. First, photothermal effects can amplify the measured optical signal. This amplification is referred to as the *enhancement factor* (Dovichi and Harris 1979; Mori, Imashaka, and Ishibashi 1982) and is the ratio of the signal obtained using photothermal spectroscopy to that of conventional transmission spectroscopy. Enhancement factors depend on the thermal and optical properties of the sample, the power or energy of the light source used to excite the sample, and the optical geometry used to excite the sample. Since the optical excitation power or energy and geometry are variable, the enhancement can be made very large, even for samples with relatively poor thermal and optical properties. In fact, the problem with photothermal spectroscopy is not the absorption detection limit. The problem is the detection of analyte absorbance in the presence of a relatively large (10^{-5} cm^{-1}) absorbance of the solvent. The second reason photothermal spectroscopy is more sensitive than transmission is that the precision of the measurement is inherently better than that of the direct transmission method. The fundamental limitation of conventional absorption spectroscopy, namely, shot noise, may

Photothermal Spectroscopy Methods, Second Edition. Stephen E. Bialkowski, Nelson G. C. Astrath, and Mikhail A. Proskurnin.

be partially circumvented (Bialkowski et al. 1992). Because of the increased fundamental signal-to-noise ratios, the problem of being able to detect the analyte in the presence of a relatively large background absorption should be able to be overcome with perseverance.

The high sensitivity of the photothermal spectroscopy methods has led to applications for analysis of low absorbance samples. Dovichi (1987) reviewed the literature regarding the use of photothermal spectroscopy for chemical analysis. The magnitude of the photothermal spectroscopy signal depends on the specific method used to detect the photothermal effect and on the type of sample being analyzed. There are many different reported detection limits, and it is difficult to specify an absolute lower limit of detection since the method may be used to measure the background absorption of the solvent itself. But it is safe to say that optical absorbances of less than 10^{-6} can be detected with optimized experimental designs. Subsequently, photothermal spectroscopy is often characterized as a trace analysis method. Concentration limit of detection measurements can be impressive. Electronic transitions of strongly absorbing chromophores have molar absorptivities exceeding $10^4\,M^{-1}\,cm^{-1}$. Using photothermal methods, concentrations lower than $10^{-10}\,M$ of these strongly absorbing chromophores may be measured in standard cuvettes. These limits of detection are slightly higher than those obtained using laser-excited fluorescence spectroscopy and are two to three orders of magnitude better than that obtained using conventional transmission spectroscopy. The low molar absorption detection limits coupled with the fact that the volume being probed can be very small result in extremely small numbers of molecules being detected. The high absorbance sensitivity of these methods has opened up new areas of trace chemical analysis based on optical absorption spectroscopy.

Photothermal signals depend on the thermodynamic and energy transfer properties of the sample. Temperature changes resulting from optical absorption are directly related to heat capacity and thermal conductivity. This makes absolute sample absorption measurements difficult. The thermal and optical properties of the sample must be known to high accuracy, or the instrument response must be calibrated with samples of known composition and absorbance. However, this dependence on thermodynamic and energy transfer properties allows for analysis of the thermal structure of materials. With calibrated apparatuses, the static and dynamic thermal properties of the sample can be measured. Photothermal spectroscopy has been used to measure acoustic velocities, thermal diffusion coefficients, sample temperatures, bulk sample flow rates, specific heats, volume expansion coefficients, and heterogeneous thermal conductivities in solids. In particular, a technique called thermal wave imaging allows nondestructive material inspection by measuring the rate of heat transfer in heterogeneous materials.

Photothermal spectroscopy is usually performed using laser light sources. There are two main reasons for this. The first is the high spectral purity and power. For an excitation of a sample with a given absorption coefficient, the temperature change will be proportional to the optical power, in the case of continuous excitation, or energy, in the case of pulsed excitation. The photothermal spectroscopy signal is generally proportional to the temperature change. Thus, the greater the power or energy, the greater the resulting signal. Lasers can deliver high powers or pulse energies over very narrow optical bandwidths, thereby enhancing the photothermal signals. The second reason is spatial coherence. The temperature change is not only proportional to the optical power or energy but also is inversely proportional to the volume over which the light is absorbed since heat capacity scales with the amount of substance. The spatial coherence properties of laser sources allow the light to be focused to small diffraction-limited volumes. The small volumes used in photothermal spectroscopy enhance signal magnitudes, allow photothermal spectroscopy to be used in small volume sample analysis, and allow for microscopic analysis of heterogeneous materials.

1.2 Basic Processes in Photothermal Spectroscopy

The basic processes responsible for photothermal spectroscopy signal generation are shown in Figure 1.1. Optical radiation, usually from a laser, is used to excite a sample. The sample absorbs some of this radiation, resulting in an increase in the internal energy. The internal energy is dispersed in two different modes of hydrodynamic relaxation. The increased internal energy results in a temperature change in the sample or the coupling fluid placed next to the sample. This temperature change results in a change in sample or coupling fluid density.

If the photothermal-induced temperature change occurs faster than the time required for the fluid to expand or in a few cases contract, then the rapid temperature change will result in a pressure change. The pressure perturbation will disperse in an acoustic wave. Once the pressure has relaxed to the equilibrium pressure, a density change proportional to the temperature will remain.

In either case there will be a change in temperature induced by the absorption of optical energy. This temperature change will in turn result in a density change in the sample. In combination, temperature and density changes affect other properties of the sample. Photothermal spectroscopy is based on a measurement of these properties. In particular, the sensitive photothermal methods are based on measurement of the refractive index change that occurs with changes in temperature and density of the sample.

There are three main areas that must be considered when attempting to obtain a quantitative description of the photothermal spectroscopy signal. The first is a description of the optical absorption and excited state relaxation processes. Optical excitation followed by excited state relaxation results in sample heating. The rates and amounts of excited state excitation and relaxation will control the rate and magnitude of heat production. The energy transfer steps that need to be accounted for are shown in Figure 1.2. Energy can be transferred to the sample by optical absorption and inelastic scattering process such as Raman. Scattering is inefficient and the amount of energy lost to sample is usually small enough to be neglected. After absorption, the molecules are in an excited state. Excited state relaxation transfers energy to the solvent or sample matrix. Radiative relaxation does not result in complete loss of the absorbed energy to the sample. Some of the energy is lost in the form of the radiated light. Thermal relaxation transfers the energy to the sample matrix and results in sample heating. Excited species may also form long-lived metastable states that trap energy and prevent further optical absorption. This will result in a delayed heating of the sample. The excited state species may also participate in photochemical reactions. Photochemical

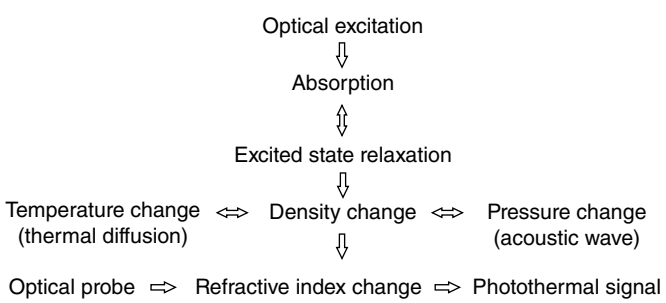

Figure 1.1 Processes involved in photothermal spectroscopy. Absorption of radiation from the excitation source followed by non-radiative excited state relaxation results in changes in the sample temperature, pressure, and density. The density change is primarily responsible for the refractive index change that can be probed by a variety of methods.

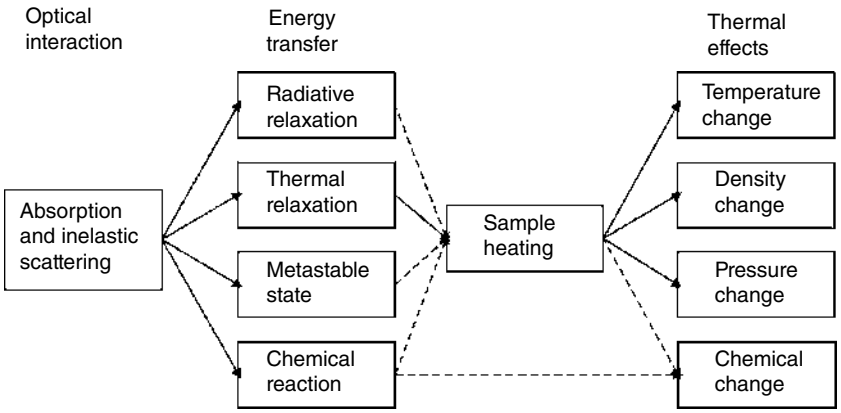

Figure 1.2 Several of the mechanisms for excited state relaxation are illustrated. The main steps are optical interaction, energy transfer, sample heating, and thermal effects. Radiative relaxation, metastable state production, and photochemical reaction may result in some sample heating. Energy transfer step may result in fast or slow kinetic energy production.

reactions not only can produce heat but can also produce new chemical species that alter the thermal and optical characteristics of the sample.

These relaxation processes may all produce excess energy in the form of heat. The heat increases the internal energy of the sample. The sample will respond to this increased energy. The second area is that of the hydrodynamic relaxation. After optical heating, the sample is not at thermal equilibrium with itself or with the surrounding environment during a measurement. Heat generated by the optical excitation and relaxation processes will result in thermal gradients between the excited sample and the surroundings. The thermal gradients result in heat transport. Heat is transferred within the sample in a fashion such as to move toward thermal equilibrium. Hydrodynamic relaxation produces changes in the temperature, pressure, and density of the sample.

The third area is that of the signal generation process. Photothermal spectroscopy signals are based on changes in sample temperature or related thermodynamic properties of the sample. These are usually monitored through the refractive index of the sample or a thermal coupling fluid placed in contact with the sample. Several properties may affect the refractive index of the medium. The most common is the density. However, the refractive index may also change with temperature, with population in optically excited states, and with chemical composition if photochemical reaction occurs. There are a variety of instrumental methods used to probe the changes in the sample's refractive index. Other instrumental methods used for photothermal spectroscopy directly probe the temperature or related thermodynamic properties, but the most sensitive methods probe the spatial or temporal gradients of these properties.

A schematic diagram illustrating the main components to apparatuses used for photothermal spectroscopy is shown in Figure 1.3. Most apparatuses consist of six main components: (i) light used for sample excitation; (ii) sample; (iii) light used to monitor refractive index perturbations; (iv) a mask, aperture, or other form of spatial filter for the probe light; (v) an optical detector used to detect the optically filtered probe light; and (vi) electronic signal processing equipment. The excitation light heats the sample. The probe light monitors changes in the refractive index of the sample resulting from heating. The spatial and propagation characteristics of the probe light will be altered by the refractive index. The spatial filter selects those components of the altered probe light that change with the samples' refractive index. The optical detector monitors changes in

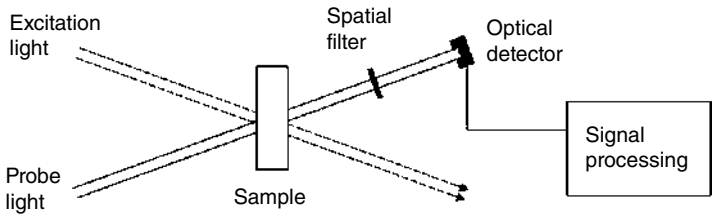

Figure 1.3 A generic photothermal spectrometer showing essential features.

the probe light power past the spatial filter. In some apparatuses, a spatial filter and a single-channel detector are combined using an image detector. Signals generated by the photodetector are processed to enhance the signal-to-noise ratio.

In addition, an apparatus may also be equipped with detectors to monitor the excitation and probe light power, a thermostatic sample holder, and optical spatial filters to control the spatial profiles of the excitation and probe light. This additional equipment is used to control the experiment environment and to measure the optical power required to accurately quantify changes that occur in the sample. These components are necessary when the data must be used to determine absolute absorption of the sample.

In theory, the photothermal spectroscopy signal can be accurately calculated based on knowledge of the experimental apparatus, the parameters that characterize light propagation, and the optical parameters of the sample. The following items must all be accounted for in the calculations: (i) determine the optical absorption resulting in sample heating, (ii) determine the rate of heat production, (iii) determine the temporal and spatial temperature and density change, (iv) relate the refractive index change to the temperature or density change using the thermal optical parameters of the sample, (v) calculate the strength of the optical element formed from the spatial-dependent refractive index change, and (vi) calculate the optical and electronic signals resulting from passage of light through apertures or using specialized detectors.

1.3 Photothermal Spectroscopy Methods

There are a variety of methods used to monitor the thermal state of the analytical sample (Harris 1986; Tam 1986, 1989; Dovichi 1987). Direct calorimetric or thermometric methods use temperature transducers to measure analytical sample temperature. Pressure transducers are used to monitor the pressure wave associated with rapid sample heating. Photothermal interferometry, photothermal deflection spectroscopy, photothermal lens spectroscopy (also known as photothermal lensing spectroscopy), photothermal diffraction spectroscopy, and methods based on sample reflection changes are all based on monitoring refractive index changes associated with sample heating. Infrared (IR) detectors can be used to monitor changes in the sample IR emission associated with heating. Each of these methods is based on a measurement of temperature change associated with increasing the energy of the analytical sample.

Photothermal methods have been reported by individuals working in several areas of science and technology. Subsequently, there are several names that the particular methods are known by. The temperature changes resulting from the photothermal effect can be detected using a variety of methods. These methods are summarized in Table 1.1. Temperature can be directly measured using thermocouples, thermistors, or pyroelectric devices in the method of *photothermal calorimetry*. Temperature changes can also be indirectly measured using methods that

Table 1.1 Common detection techniques used in photothermal spectroscopy.

Thermodynamic parameter	Measured property	Detection technique
Temperature	Temperature	Calorimetry
	Infrared emission	Infrared emission
		Photothermal radiometry
Pressure	Acoustic wave	Photoacoustic spectroscopy
Density	Refractive index	Photothermal lens
		Photothermal interferometry
		Photothermal deflection
		Photothermal refraction
		Photothermal diffraction
	Surface deformation	Photothermal deflection
		Photothermal mirror

monitor IR emission since the thermal IR emission is related to sample temperature. The method of *thermal emission* or *photothermal radiometry* (PTR) of IR radiation can be used to monitor relatively large temperature changes that occur as a consequence of optical absorption. Although not very sensitive, this method has great potential for application in nondestructive materials analysis and testing. Using IR sensitive cameras, it can be used for imaging the thermal properties of large samples.

Two other temperature-dependent thermodynamic parameters that are commonly exploited in photothermal spectroscopy are pressure and density. The pressure changes that occur upon periodic or pulsed sample heating can be detected by using a microphone or other pressure transducer to monitor the acoustic wave. The method of optoacoustic or *photoacoustic spectroscopy* is based on the measurement of this pressure wave.

Although produced by the same photothermal effects, photoacoustic, IR radiometry, and photothermal spectroscopies are typically treated as separate methods. Photothermal spectroscopy refers to methods that monitor the temperature-dependent refractive index changes, usually with a probe laser. Nonetheless, it is apparent from hydrodynamic relaxation that the photoacoustics cannot be avoided in a treatment of photothermal spectroscopy. The photoacoustic pressure wave generated by the photothermal effect is observed in photothermal spectroscopy, and the rate of sample relaxation is controlled by the rate at which the sample can approach isobaric conditions. Moreover, IR emission is another method of thermal heat transfer that should at least be quantified in terms of the effect that it may have on the photothermal signal magnitude. All of these effects should be considered in a comprehensive treatment of the photothermal effect.

Under steady-state isobaric condition, the density is related to the temperature through the volume expansion coefficient. Temperature-dependent density changes are difficult to measure directly. But density changes can affect samples in several different ways. In solid samples, the density change alters physical dimensions at sample surfaces. Sample dimension changes give rise to two optical methods for monitoring the temperature change based on surface deformation. A homogeneous deformation (expansion or contraction) displaces the surface of the sample. Interferometry can be used on reflective samples. Since small displacements, on the order of a few parts per million of the wavelength of probe beam light, can be measured using interferometry, this method may be used for sensitive measurement solid sample absorption. Spatially heterogeneous expansion (or contraction) can also cause the surface angle to change. A probe beam reflected from the surface will change angle when heterogeneous expansion occurs.

Measurement of the probe beam angle gives rise to the method of *photothermal surface deflection spectroscopy*. Measurement of the probe beam focusing or defocusing gives rise to the method of *photothermal mirror (PTM) spectroscopy*.

The majority of studies addressing the use of photothermal spectroscopy for chemical analysis have been based on refractive index measurements. In transparent samples, the temperature-dependent refractive index of the sample itself is probed. For opaque or scattering surfaces, temperature-dependent changes in the refractive index of fluid that couples heat out of a solid sample are measured. There are several methods used to detect the resulting refractive index or optical path change. Several of these are shown in Figure 1.4. Publications in photothermal spectroscopy come from researchers working in the fields of analytical and physical chemistry, physics, and optical engineering. Subsequently there is a wide range of nomenclature used to describe methods for refractive index change detection in the photothermal spectroscopy literature. But all of these methods rely on a few basic principles of light propagation, namely, optical path length changes, diffraction, and refraction. Light refraction can result in a direction change and/or focusing/defocusing.

The optical path length changes that occur due to the photothermal-induced refractive index change can be measured with interferometry. Using interferometry, the phase of monochromatic light passing through the heated sample, relative to the phase passing through the reference arm, results in a change in power at a photoelectric detector. There are several different interferometric schemes that can be used to detect changes in the optical path length induced by the photothermal effect. These methods may all be classified as being *photothermal interferometry*.

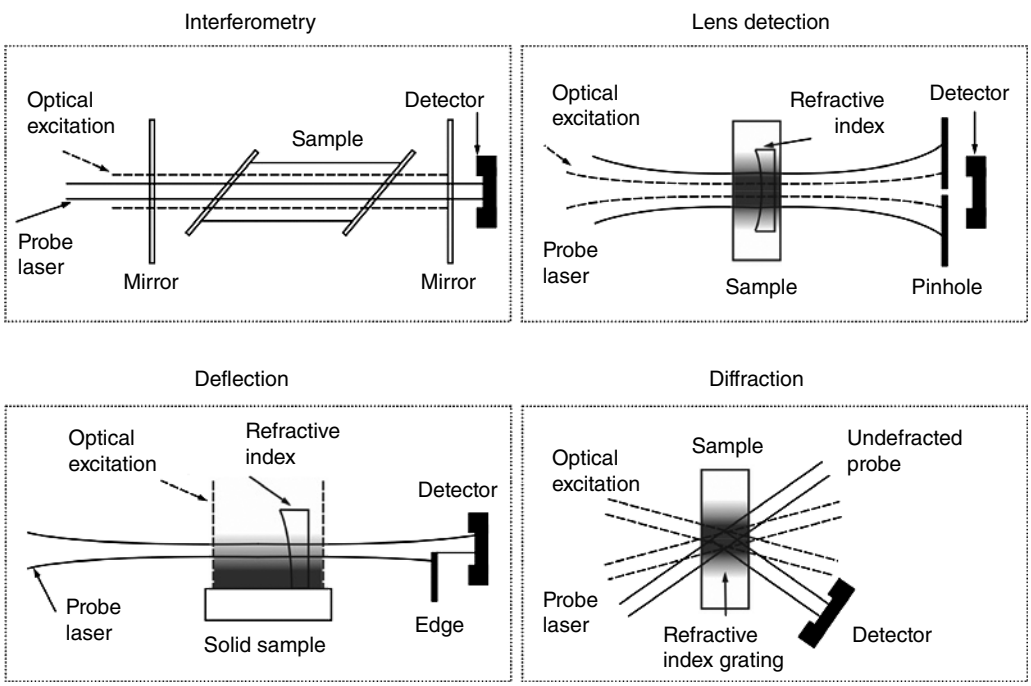

Figure 1.4 Four methods used for photothermal spectroscopy. Interferometry directly measures the refractive index. Deflection measures the gradient. Photothermal lens spectroscopy is based on beam focusing or defocusing. Diffraction methods measure the power of a beam diffracted by the periodic index.

Spatial gradients in refractive index result in a direction change in the propagation of a ray of light. Thus light will exit a medium with a refractive index gradient at an angle relative to the incident ray. This bending of light path is commonly called *photothermal deflection spectroscopy*.

Spatial-dependent refractive index profiles can also result in focusing or defocusing of light. This occurs when the refractive index profiles are curved. Thus, the thermally perturbed sample can act as a lens. Light transmitted through an aperture placed beyond the photothermal lens will vary with the strength of the lens. Photothermal methods based on measurement of the strength of this lens are called *photothermal lens spectroscopy*. Some experimental apparatuses measure a signal that is due to the combined effects of deflection and lensing. These may be generally classified as *photothermal refraction spectroscopy* methods.

Lastly, a periodic spatial refractive index modulation results in a volume phase diffraction grating. The grating will diffract light at an angle that meets requirements from Bragg's law. The amount of light diffracted is proportional to the refractive index change. The diffracted light is measured with a photoelectric detector. Methods used to measure spectroscopic signals based on volume phase diffraction gratings formed by the photothermal effects are called *photothermal diffraction spectroscopy*.

The key to the success of sensitive photothermal apparatuses lies in measurement of a thermal *change* and not the thermal state itself. Although apparatuses could directly or indirectly measure the thermodynamic parameters such as temperature, pressure, density, and energy state, the limiting absorption that could be measured would be imposed by thermodynamic fluctuations. Sensitive photothermal spectroscopy methods circumvent direct measurements by measuring refractive index changes due to a nonequilibrium change in the energy of the sample. The change occurs in both space and time. Photothermal spectroscopy methods measure some effect that the spatially or temporally dependent refractive index change has on the propagation characteristics of light used to monitor the refractive index.

Each of these apparatuses detects the change in refractive index that accompanies optical absorption. Photodetectors are used to monitor probe power changes. These power signals are time dependent. The analytical signal is usually related to the change in detected power relative to the incident power of the probe. There are three main types of time dependence that analytical signals can have. These in turn depend on the temporal character of the excitation source. The main excitation and detection schemes are given in Table 1.2.

Pulsed excitation sources produce transient signals. These signals are at a maximum immediately following sample excitation and decay as the sample approaches equilibrium through thermal diffusion. The transient signals last from a few microseconds in the gas phase to several milliseconds in condensed phases. The time duration is inversely proportional to the thermal conductivity of the media since thermal diffusion or conduction removes energy from

Table 1.2 Main sample excitation schemes used in photothermal spectroscopy.

Excitation	Signal	Detection
Pulsed	Short-lived transient; magnitude decreases with time	Peak magnitude estimation and transient waveform analysis
Continuous	Long-lived transient; magnitude increases with time	Steady-state magnitude estimation and transient waveform analysis
Modulated	Periodic modulation; magnitude and phase are functions of frequency	Periodic wave magnitude and phase analysis using frequency selective filters or lock-in amplifiers

the sample and more importantly distributes the energy throughout the sample. Photothermal lens, deflection, and diffraction apparatuses respond to spatial variations in the refractive index. Thus, homogeneous distribution of energy throughout the sample does not result in a signal. Interferometric measurements may be able to detect the refractive index change after thermal diffusion has distributed the energy. However, environmental thermal stability is usually not good enough to allow this. Sensitive interferometric apparatuses rely on the detection of a temporal change in refractive index.

Continuous excitation produces signals that are initially small but increase in magnitude as the irradiation time progresses. Initially, thermal diffusion removes heat slower than the heat produced by optical excitation. The Fourier law of heat diffusion states that the heat flux, $\mathbf{j}_H$, is proportional to the temperature gradient:

$$\mathbf{j}_H = -\kappa \nabla T \tag{1.1}$$

The proportionality constant is the thermal conductivity κ. As the sample absorbs radiation and converts the energy to heat, the temperature gradient increases. When the radiative heating flux equals the energy flux due to thermal conduction, a steady-state spatially dependent temperature change is attained. Thus the photothermal signals eventually reach a steady-state value. The signals develop over the course of from milliseconds to seconds, the time required to attain the steady-state value being proportional to the thermal conductivity.

For analytical, e.g. concentration, measurements, both pulsed and continuous excitation requires estimation of the signal magnitude. Signal magnitudes are directly proportional to the sample absorbance in a first-order approximation. Signal magnitudes can be measured directly, for example, using an oscilloscope or ammeter, or the signal transient can be recorded and subsequently processed to enhance measurement precision.

Excitation sources may also be modulated. Chopped or oscillatory excitation produces oscillating signals. The resulting signals can be processed using band-pass filters or lock-in amplifiers. The magnitudes of the oscillating signals depend on sample absorbance, the frequency of excitation, and thermal conductivity of the medium. With modulated excitation, signal magnitudes are proportional to sample absorbance but decrease with increasing frequency. In addition to the signal amplitude information, phase-sensitive lock-in analyzers also produce signal-to-excitation phase shift information. The frequency-dependent phase shift information is essentially equivalent to that contained in the time-dependent signal transients obtained using pulsed excitation.

1.4 Application of Photothermal Spectroscopy

There have been many applications of photothermal methods for chemical and materials analysis. Tam (1983, 1986, 1989) is perhaps primarily responsible for sorting through the vast amount of literature and characterizing the applications of these methods. Many of these applications are covered in the book edited by Sell (1989). These applications fall under four main categories:

1) *Photothermal spectroscopy*: The signal magnitude is measured as a function of wavelength in this application. The photothermal signal is proportional to the absorbed light. So the spectrum is technically an excitation spectrum. The resulting excitation spectrum can be an accurate measure of the absorption spectrum if the thermal quantum yield and fraction of light transmitted to the absorber do not change with wavelength. This technique has found widespread use for solid sample analysis where incoherent excitation light sources can be

used. Applications to liquid and gas sample analysis have been limited because of the difficulties encountered when attempting to scan the wavelengths of lasers while keeping them focused at a particular position.

2) *Photothermal detection*: It is similar to photothermal spectroscopy, except a single wavelength source is used to excite the sample. The signal magnitude can be related to sample absorbance or analyte concentration. Samples must be prepared and separated so that there is no interference absorption and so that the sample matrix is the same for all measured samples. The main application is for trace analysis. Although not restricted to coherent sources, this application is normally performed using laser excitation sources to enhance the limits of detection. The application is also suited for effluent detection in chromatography. The spatial coherence of lasers allows the use of small volume detection cells or on-column detection.
3) *Photothermal monitoring of excitation and relaxation process*: In this application the signal magnitude is measured as a function of time or excitation irradiance. The time-dependent data is used to deduce photophysical and photochemical parameters such as excited state lifetimes, enthalpies of formation, lifetimes of metastable states, and thermalization times. The excitation irradiance-dependent data can be used to calculate multiphoton absorption cross sections and parameters relating to optical saturation and bleaching.
4) *Photothermal probing of physical properties*: Many of the physical properties of a sample can be determined using photothermal methods. Photothermal methods have been used to measure temperature, thermal diffusivities, sound velocity, bulk flow velocities, surface thickness, and specific heats. In homogeneous samples, the full photothermal transient is typically analyzed in order to obtain this information. However, some of these parameters can be determined by measuring signal magnitudes, signal decay times, and signal onset times for carefully designed experiments. Thermal properties of heterogeneous samples can be obtained by raster scanning the optical excitation source over the sample surface. In this case the signal magnitude and phase is measured as a function of spatial coordinate.

1.5 Illustrative History and Classification of Photothermal Spectroscopy Methods

1.5.1 Nature of the Photothermal Effect

Most of us observe the photothermal effect in our lives. On the beach, sand is too hot to walk on with bare feet in midday summer. This is because the sand absorbs the sun's radiation and converts this energy to heat. The added heat results in a temperature increase because of the finite heat capacity of the sand. When heat is generated faster than it can be dissipated by radiative or diffusive mechanisms, the temperature of the sand increases. However, the rate of heat dissipation increases with the temperature difference between the surface sand and soil below or air above it. Under constant illumination conditions, the sand reaches an equilibrium temperature wherein the rate of heat generated by the photothermal effect is balanced by the rate at which the heat is dissipated. Another way we utilize the photothermal effect is to warm ourselves by the radiation of a campfire. Here, our skin is the absorber and the campfire is the source of the IR radiation.

A concrete example of the photothermal effect, which is also the basis for a photothermal spectroscopy method, is the shimmering surface or optical mirage effect. This effect is illustrated in Figure 1.5. A hot highway sometimes looks like a reflective surface. It appears as if it were a puddle of water. We come to understand that the apparently shiny surface is not due to

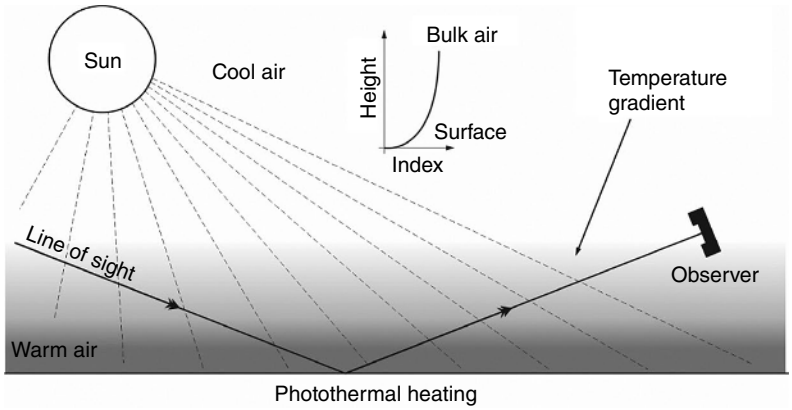

Figure 1.5 A simple photothermal deflection apparatus for measuring absorbance of the Earth's surface. Since the signal depends on meteorological and solar conditions, in this measurement it is difficult to obtain accurate numbers.

reflection. It is just a mirage. In fact, the mirage effect is one of the photothermal effects that have been exploited for chemical and materials analysis. Radiation from the sun is absorbed by the concrete or asphalt resulting in surface heating. The hot surface transfers energy to the air above the surface. A temperature gradient develops between the air near the surface and the bulk air above. Air expands when it is heated. The density of the air at the surface is less than that in the bulk. The decreased density results in a decreased refractive index. Since the speed of light is faster in the low refractive index media, light incident at an acute tangent angle is refracted upward. An observer looking at the surface at an acute tangent angle does not see the surface but rather sees the rays coming from the sky above the surface.

It is likely that our predecessors had a working knowledge of the photothermal effect long before they could apply more abstract concepts such as optical transmission, color, and other factors leading to modern theories of spectroscopy. But although photothermal effects may have been recognized in the prehistoric past, it took an understanding of the photothermal process to apply the photothermal effect for spectrochemical measurements. Much of what is now known about photothermal spectroscopy has been developed over the past century. Many of the advances came about as a result of the developments in laser technology. Other advances were made simple by the recognition and understanding of what is now called the photothermal effect.

1.5.2 Photoacoustic Spectroscopy

The oldest technical application of the photothermal effect is believed to be the communication device, the photophone, invented by Bell (1880, 1881). Bell found that audible sound could be heard coming from a tube filled with various materials when the light shining on the transparent tube was modulated. The sound was loud when the tube was filled with radiation-absorbing gases or solids and weak when filled with a liquid. The operational principles are now well understood. Modulation of the light impinging on an absorbing substance will produce a similar modulation in temperature through the photothermal effect. In a gas of restricted volume, temperature modulation produces a pressure modulation. The periodic pressure modulation is an acoustic signal.

Some time later Viengerov (1938) used the photoacoustic effect to study light absorption in gases and obtained quantitative estimates of concentration in gas mixtures based on signal magnitudes. This may have been the first use of photoacoustic spectroscopy. Sensitive chemical measurement applications followed the work of Kerr and Atwood (1968) who used a laser to excite the samples. More interest in the method was generated when Kreuzer (1971) demonstrated part-per-billion (ppb) detection sensitivities of methane in nitrogen using a 3.39 μm helium–neon laser excitation source and later (Kreuzer, Kenyon, and Patel 1972) sub-ppb of ammonia and other gases using IR CO and CO_2 lasers. These high sensitivity measurements were possible because of the laser source used for excitation. Large photoacoustic spectroscopy signals resulted from the high spectral brightness and the spatial coherence of the lasers used for sample excitation. The photoacoustic measurement methods came at about the same time as the recognition that trace species could have a major impact on the environment.

In the time since the first chemical measurements by Viengerov (1938), theory and practice has been developed to a high degree. The theories for sound generation, propagation, and interaction with matter were developed through the mid-twentieth century (Herzfeld and Litovitz 1959; Landau and Lifshitz 1959), and acoustics were applied to physical–chemical analysis. The theories are complex and exact solutions for sample excitation and signal generation are often difficult to interpret and verify. Nonetheless, the principles of photoacoustic spectroscopy are now commonly understood, and photoacoustic spectroscopy is being applied to a wide range of analysis problems.

The essential components for an apparatus used for photoacoustic spectroscopy are shown in Figure 1.6. The light source, either pulsed or modulated, periodically heats the sample by the photothermal effect. Periodic sample heating followed by expansion causes a periodic pressure wave that is detected with the pressure transducer. The pressure transducer signal is proportional to the amplitude of the pressure wave. Consider a sample that has a low enough absorption coefficient that the transmission can be approximated by

$$T(l) = e^{-\alpha l} \approx 1 - \alpha l \tag{1.2}$$

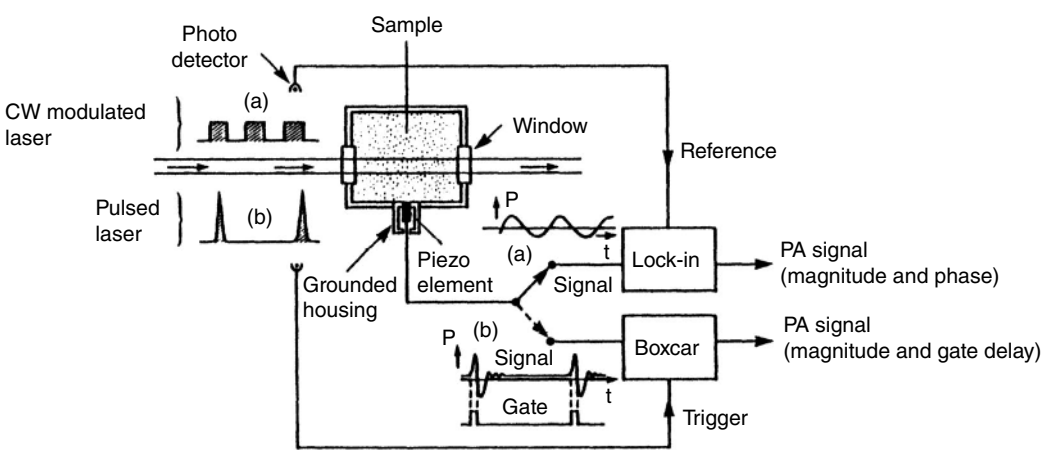

Figure 1.6 Schematic of a photoacoustic spectrometer based on direct acoustic wave detection. Chopped (a) or pulsed (b) sample excitation results in acoustic pressure wave generation. The signal is detected with a piezoelectric pressure transducer and processed with either a lock-in or sampling (boxcar) amplifier. Source: From Tam (1989). Reproduced with permission of Elsevier.

where $T(l)$ is the optical path length, l (m) is the dependent transmission, and α (m^{-1}) is the absorption coefficient. The amount of energy absorbed from a laser source with an optical energy of Q (J) is $Q[1 - T(l)] \approx Q\alpha l$. If the quantum yield for heat production is unity, all the absorbed optical energy is converted into heat. The peak pressure change, $\delta P_{acoustic}$ (Pa), is proportional to (Lai and Young 1982; Tam 1986) $\tau^{-3/2}(\alpha\beta Q/C_P)$ $(c/r)^{1/2}$:

$$\delta P_{acoustic} \propto \tau^{-3/2} \frac{\alpha\beta Q}{C_P} \left(\frac{c}{r}\right)^{1/2} \tag{1.3}$$

where c ($m\,s^{-1}$) is the sound velocity, β (K^{-1}) is the volume expansion coefficient, r (m) is the radial distance between the transducer and the source, C_P ($J\,kg^{-1}\,K^{-1}$) is the specific heat, Q (J) is the pulse energy, and the pressure perturbation time, τ (seconds), is the root-mean-square average of the relaxation times and the pulse or modulation width. Relaxation times may include contributions from the excited state relaxation time and the acoustic relaxation time:

$$\tau_a^2 = \frac{w^2}{2c^2} \tag{1.4}$$

where τ_a (seconds) is the acoustic relaxation time and w (m) is the radius of the beam used for sample excitation. The acoustic relaxation time is that required for the heated sample to expand.

The important points to be deduced from the acoustic pressure equation are as follows: (i) The signal scales as the αQ product. (ii) The signal falls off as the pressure transducer is moved away from the excited region as $r^{-1/2}$. (iii) The signal is inversely proportional to the pressure perturbation time, favoring short pulse excitation and small beam waists. (iv) The signal magnitude is proportional to the thermodynamic properties of the sample through the $(\beta c^{1/2}/C_P)$ term. In general, β is much smaller for liquids and solids than it is for gases. Not only does this explain the early observations of Bell (1881) but also explains why direct photoacoustic spectroscopy is most sensitive for gas sample analysis.

The spectra of solid or liquid samples can be measured by directly coupling the acoustic wave to a transducer or by coupling the heat generated at the surface to a gas "coupling fluid." This principle was used in Bell's original photophone but was not rediscovered until Parker (1973) noticed that optical energy absorbed by the gas sample cell windows would transfer heat to a gas, thereby causing a significant photoacoustic signal. This effect was developed by Rosencwaig (1977, 1980) and is now commonly used for obtaining spectra of strongly absorbing solids and liquids. A modern version of a device for photoacoustic spectroscopy of condensed samples is shown in Figure 1.7. A solid or liquid sample is placed in the sealed photoacoustic cell. The excitation source is absorbed at or near the surface. Absorbed radiation is randomized increasing the surface temperature. The heated surface heats the gas causing it to expand. Periodic heating of the surface creates an acoustic wave that is monitored with the sound transducer.

There have been scores of publications on the uses of photoacoustic spectroscopy for chemical and materials analysis. Absorption detection limits (α) are about 10^{-10} cm^{-1} for gases (Patel, Kerl, and Burkhardt 1977) and 10^{-6} cm^{-1} for liquids (Beitz et al. 1990). These are very close to the theoretical detection limits (Zharov and Letokhov 1986). Many review articles and books have been written on this method. Some of the reviews of general applications are Tam (1983, 1986) and Hutchins and Tam (1986). Patel and Tam (1981) reviewed applications of photoacoustic spectroscopy for condensed matter. Betteridge and Meylor (1984) have reviewed the applications of photoacoustic spectroscopy in chemical analysis. Zharov (1986) reviewed photoacoustic applications to chromatography. Meyer and Sigrist (1990) have reviewed applications to gas analysis. General books on photoacoustic spectroscopy include

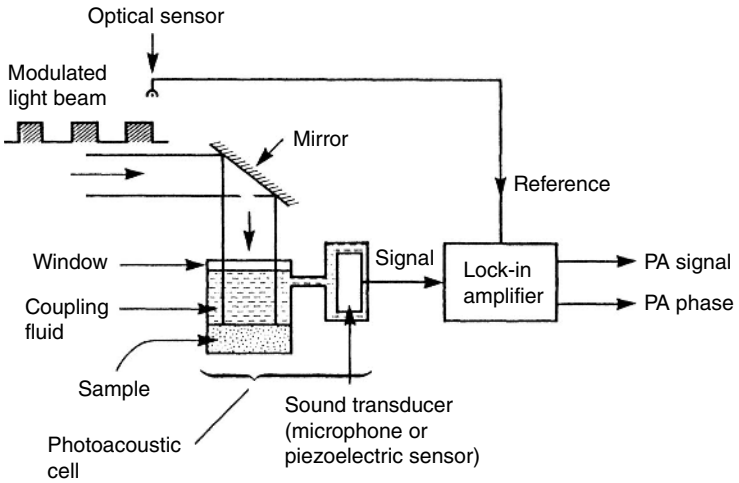

Figure 1.7 Schematic of an indirect photoacoustic spectrometer based on chopped excitation. The thermal perturbation generated in the sample is coupled to the fluid, usually a gas, and sensed with the microphone pressure transducer. The microphone signal is then processed with a lock-in amplifier to enhance the signal. Source: From Tam (1989). Reproduced with permission of Elsevier.

those of Pao (1977), Rosencwaig (1980), and Zharov and Letokhov (1986). Mandelis (1987) has edited a book on the application of photoacoustic and photothermal spectroscopy methods to semiconductor analysis. Hess (1989a, b) has edited books regarding the application of photoacoustic and photothermal spectroscopy methods for gas and surface analysis. Nyquist et al. (1990) and Putzig et al. (1990) have reviewed photoacoustic and photothermal spectroscopies in their *Analytical Chemistry* "Fundamental Reviews" of IR analysis. Kitamori and Sawada (1991) have discussed unconventional applications in their review.

1.5.3 Single-Beam Photothermal Lens Spectroscopy

The first photothermal spectroscopic method to be applied for sensitive chemical analysis was photothermal lens spectroscopy. The photothermal lens effect was discovered when Gordon et al. (1964, 1965) observed transient power and beam divergence changes in the output of a helium–neon laser after placing "transparent" samples in the laser cavity. Their apparatus, shown in Figure 1.8, was originally intended to be used as a high irradiance source for Raman spectroscopy. They observed the photothermal lens effect when pure organic liquids and solids, such as glass and Lucite, were placed in the laser cavity. A theory describing the effect was developed to account for their observations. This theory was an accurate description of the physics of photothermal lens formation and signal generation and is essentially the same as that used to this day (Whinnery 1974). The photothermal lens results from optical absorption and heating of the sample in regions localized to the extent of the excitation source. The lens is created through the temperature dependence of the sample refractive index. The lens usually has a negative focal length since most materials expand upon heating and the refractive index is proportional to the density. This negative lens causes beam divergence and the signal is detected as a time-dependent decrease in power at the center of the beam.

Laser output power transients for the first apparatus are shown in Figure 1.9. Although the theory was accurate, these transients were difficult to interpret. The transients arose due to

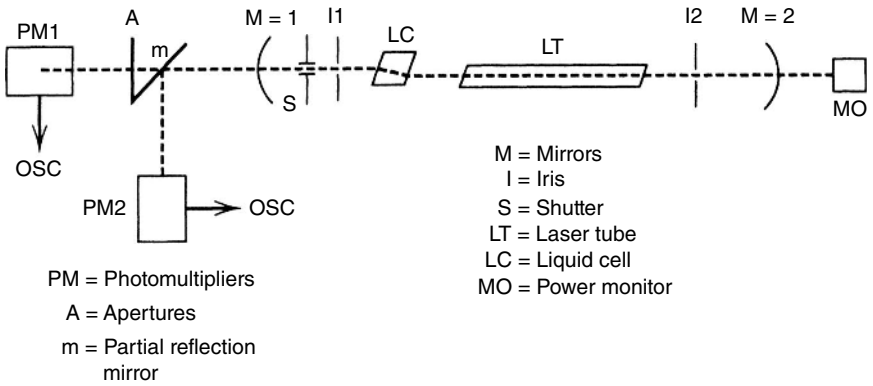

Figure 1.8 First photothermal lens apparatus. The sample was placed in the cavity of the laser. Irises were used to restrict the laser to single TEM_{00} mode operation. Detectors were used to measure the laser power and the laser output both with and without an external pinhole. Source: Reprinted from Gordon et al. (1965), with the permission of AIP Publishing.

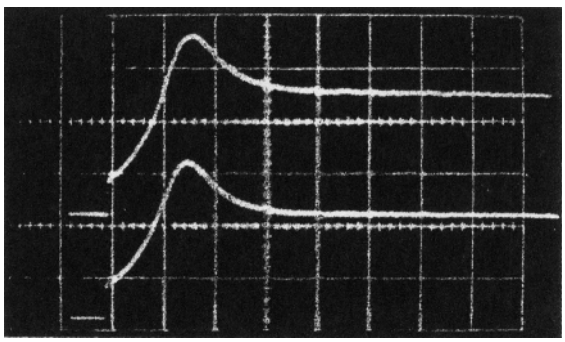

Figure 1.9 Transient signals observed using the intracavity photothermal lens apparatus. The top trace was obtained with an extracavity pinhole and the bottom trace was obtained without the pinhole. This data was used to confirm the premise that the laser was operating in single mode and that the signal was generated by the internal apertures. These signals were difficult to analyze because of the interrelationships between laser power and cavity losses. Source: Reprinted from Gordon et al. (1965), with the permission of AIP Publishing.

the interaction between the intracavity beam propagation altering character of the photothermal lens element and the intracavity apertures. Nonetheless, Solomini (1966) refined the apparatus and measured the absorption coefficients of 27 organic liquids using this method.

The first extracavity sample photothermal lens apparatus was used by Grabiner, Siebert, and Flynn (1972) to measure vibrational relaxation rate constants. Hu and Whinnery (1973) recognized that the extracavity sample configuration would be more flexible and could also result in sensitive absorbance measurements. The apparatus and beam analysis, shown in Figure 1.10, are essentially the same as that used for single-laser photothermal lens spectroscopy today. The transient signals produced extracavity are less complicated than those of the intracavity configuration, and the theory describing the transients is more tractable. The essential components of the apparatus are (i) the coherent laser excitation source, which can deliver high optical powers over a small cross-sectional area of the sample; (ii) a low absorbance sample; (iii) a spatial filter or pinhole placed in the far field; and (iv) a photodetector to measure the power past the pinhole.

The extracavity photothermal lens spectroscopy signal can be described in terms of the focal length of the photothermal lens formed within the sample. The simplest form of the focal length

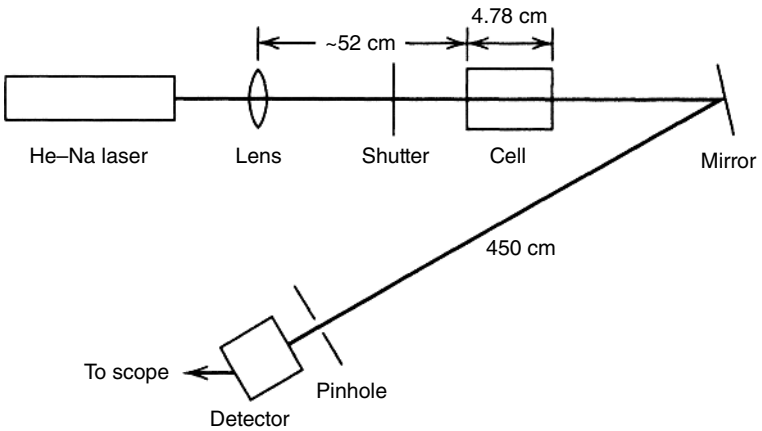

Figure 1.10 A schematic of the extracavity photothermal lens spectrometer used by Hu and Whinnery (1974) to measure the optical absorbances in transparent fluids. The lens focuses the laser beam one confocal distance in front of the sample cell. The pinhole and detector are placed in the far field of the focus. Source: Reprinted (adapted) with permission from Whinnery (1974). Copyright 1974 American Chemical Society.

is found by assuming that $\alpha l \ll 1$ and unit quantum efficiency for heat production. A sample excited by a laser beam with an irradiance of

$$E(r) = \frac{2\Phi_0}{\pi w^2} e^{-2r^2/w^2} \tag{1.5}$$

where $E(r)$ (W m^{-2}) is the radially dependent irradiance and Φ_0 (W) is the incident radiant power will produce a time-dependent photothermal lens with a focal length, $f(t)$:

$$f(t) = f(\infty)\left(1 + \frac{t_c}{2t}\right) \tag{1.6}$$

where $f(\infty)$ (m) is the steady-state focal length formed at infinite time

$$f(\infty) = \frac{n_0 \pi \kappa w^2}{\Phi_0 \alpha l (dn/dT)} \tag{1.7}$$

and t_c (seconds) is the characteristic thermal time constant

$$t_c = \frac{w^2 \rho C_P}{4\kappa} \tag{1.8}$$

where κ (J cm^{-1} s^{-1} K^{-1}) is the thermal conductivity, n_0 is the refractive index of the medium where detection takes place (normally air), n is the refractive index of the sample, T (K) is the temperature, ρ (kg m^{-3}) is the density, and C_P (J kg^{-1} K^{-1}) is the specific heat. The lens is formed because the optically heated sample has a different refractive index from that of the bulk of the sample. The differential term $(dn/dT)_P$ is the temperature-dependent refractive index change at constant pressure. The shape of the temperature change produced by a Gaussian excitation source is parabolic near the center. The parabolic refractive index perturbation is equivalent in form to a simple lens.

The photothermal lens signal is obtained by monitoring the laser power that passes through a pinhole placed far from the sample. The photothermal lens will either focus or defocus the laser.

When this happens, the power at the center of the beam will either increase or decrease. This change in power is maximized when the sample is placed one confocal distance to either side of the laser's focus. In this case the relative change in power monitored past the pinhole either focuses or defocuses the laser. When this happens, the power at the center of the beam will either increase or decrease. This change in power is maximized when the sample is placed one confocal distance to either side of the laser's focus. In this case the relative change in power monitored past the pinhole aperture is

$$\frac{\Phi_d(0)-\Phi_d(t)}{\Phi_d(t)} \approx \frac{\pm 2z_0}{f(t)} \tag{1.9}$$

where $\Phi_d(t)$ is the time-dependent power and the confocal distance is $z_0 = n_0\pi {w_0}^2/\lambda$, w_0 being the beam waist radius at the focus, and λ (m) is the wavelength of the laser. The + sign applies to samples placed before the focus, and the – sign for samples behind the focus. The time-dependent signal observed past the pinhole is

$$\frac{\Phi_d(0)-\Phi_d(t)}{\Phi_d(t)} \approx \pm\left(\frac{dn}{dT}\right)\frac{\alpha l \Phi_0}{\lambda\kappa}\frac{1}{1+t_c/2t} \tag{1.10}$$

The essential components to interpreting the signal are the following: (i) The time-dependent signal increases or decreases the power past the pinhole. (ii) The time constant for signal evolution, t_c, is proportional to the square of the beam waist radius in the sample. (iii) The signal magnitude is proportional to the absorption coefficient, path length, and excitation power. (iv) The signal magnitude also depends on the thermal, κ, and optical, (dn/dT), properties of the sample. (v) For times much greater than t_c, the steady-state power change is related to absorption coefficient by

$$\pm\alpha \approx \frac{\Phi_d(0)-\Phi_d(\infty)}{\Phi_d(\infty)}\frac{\lambda\kappa}{\Phi_0 l(dn/dT)} \tag{1.11}$$

The absorption coefficient can be obtained by measuring the power change with knowledge of the temperature-dependent refractive index (Figure 1.11).

It is difficult to see from these equations how the photothermal lens spectroscopy method can enhance absorbance measurements. Dovichi and Harris (1979) introduced the concept of the enhancement factor. The enhancement factor is the ratio of the photothermal lens signal magnitude to that which would be obtained using conventional transmission spectroscopy.

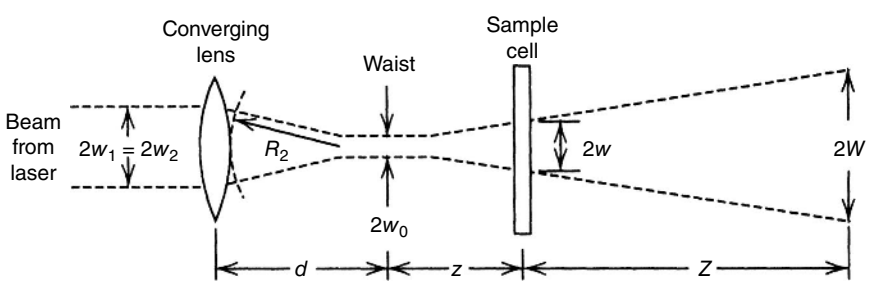

Figure 1.11 Illustration of the beam geometry and definitions used for extracavity photothermal lens spectroscopy. Source: Reprinted (adapted) with permission from Whinnery (1974). Copyright 1974 American Chemical Society.

For weakly absorbing samples, the transmission spectroscopy signal can be cast in a form similar to that for the photothermal lens spectroscopy signal:

$$\frac{\Phi_0 - \Phi_l}{\Phi_0} \approx \alpha l \tag{1.12}$$

where Φ_l is the power after passing through the sample. The ratio of the photothermal lens signal to this signal yields the enhancement factor

$$E = \left(\frac{dn}{dT}\right)_P \frac{\Phi_0}{\lambda \kappa} \tag{1.13}$$

The enhancement is a function of the thermodynamic and optical properties of the solvent and of the power used to excite the sample. Nonpolar solvents are particularly useful for trace analysis because of their relatively high $(dn/dT)_P$ and low κ. For example, CCl_4 has temperature-dependent refractive index of -6.12×10^{-4} K^{-1} and a thermal conductivity of 0.103 W m^{-1} K^{-1} (Dovichi 1987). The theoretical enhancement factor is 11 560 W^{-1} for the 514 nm line of an argon ion laser. Of course, higher laser power produces a greater enhancement. Even a modest 10 mW laser will yield signals that are over 100-fold better than those of the conventional transmission spectrophotometer. Absorption coefficient detection limits in 1 cm cuvettes are about 10^{-7} cm^{-1}. This detection limit was reported by Dovichi and Harris (1981) for 514.5 nm excitation of samples in CCl_4 solvent using 160 mW of laser power. The enhancement factor under these conditions is approximately 1850. Based on these, the absorbance detection limits calculated for the equivalent conventional transmission spectrophotometer would be 2×10^{-4} absorbance units. Although it is a matter for discussion, this is about what one might expect from a double dispersing transmission spectrophotometer.

The characteristic time constant, t_c, should also be considered in the experimental design. With a shorter time constant, more measurements can be made in a given time. Since replicate measurements can be used to increase the precision of the estimate, the shorter time constant resulting from smaller focus spot sizes is favored. For example, CCl_4 has a thermal diffusivity of 7.5×10^{-8} m^2 s^{-1}. A laser with a beam waist radius of 1 mm in the sample cell will produce a signal with a characteristic thermal time constant of 3.3 seconds, whereas using a 10 μm beam waist radius, t_c = 0.33 ms. The 10 μm beam would allow 10^4 replicate measurements in the same time required to obtain one measurement with a 1 mm beam waist. The measurement precision would increase by 100 using the smaller beam waist and equivalent measurement times.

The first analytical application of photothermal spectroscopy was the trace level determination of Cu(II) with an EDTA complex reported by Dovichi and Harris (1979). They used the single-laser extracavity photothermal lens apparatus. This method is perhaps the most well known and used of all the photothermal spectroscopy methods. The relative simplicity of the apparatus coupled with the low solution absorption detection limits, 10^{-7} cm^{-1} (Dovichi and Harris 1981), makes it highly attractive for trace analysis applications.

1.5.4 Photothermal *Z*-scan Technique

Z-scan is a selection of highly sensitive techniques for determining optical properties of various materials (Sheik-Bahae et al. 1990), the main requirement for the materials under investigation being transparency, but also in a highly dispersive medium (Olivares et al. 2005). A test sample is moved through the focus of a laser beam along the beam propagation axis, and the beam radius or the on-axis irradiance (normalized transmittance) as a function of the sample position is measured by a detector placed at some plane behind the focus. This function is affected by

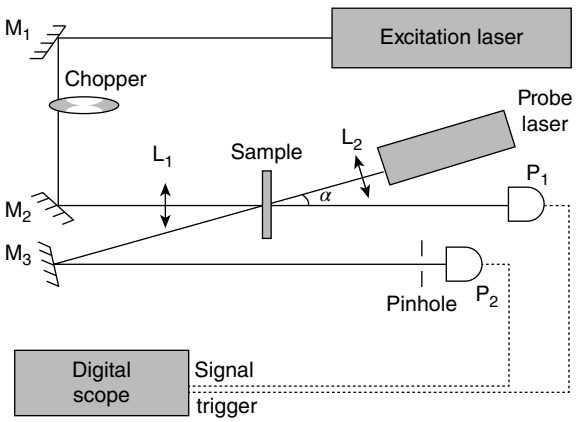

Figure 1.12 Schematic diagram of the *z*-scan mode mismatched thermal lens apparatus for measuring nonlinear optical properties of materials, where M's are mirrors, P's are photodetectors, and L's are convergent lenses. (Upper) Lens effect in the *Z*-scan technique for the case of complex nonlinear refractive index $n_2 > 0$. (i) Before the beam waist, the induced focus spreads the light on the detector. (ii) After the beam waist, the light is focused on the detector. (iii) Characteristic transmittance curve for a positive nonlinearity. Source: Jacinto et al. (2006). Reproduced with permission of Elsevier.

the self-focusing and self-defocusing effects in the material – optical Kerr effect, electrostriction, two-photon absorption, and photothermal phenomena. It allows unambiguous calculation of the real and imaginary parts of the optical absorption function of the material, as well as the study of nonlinear optical properties of the sample (Mian, McGee, and Melikechi 2002). A schematic diagram of the technique is shown in Figure 1.12.

The observed dependences are based on the transition from the minimum refraction of the beams (the sample is far from the waist of the laser beam; the energy of the beams is minimal) to the situation when the increase in the radiation fluence and the formation of the photothermal lens element in the sample begin to play a significant role in the propagation of the beam (Sheik-Bahae et al. 1990). For a material with negative nonlinear refraction, the negative lens to the point of focus will have a collecting effect, increasing the irradiance transmitted through the pinhole in the plane of the detector. After passing through the focus of the beam, the formed lens amplifies the divergence of the beam, further reducing its irradiance in the plane of the detector. Thus, a sample with a negative nonlinear refractive index will have a maximum on the curve followed by a minimum (when moving from the lens to the detector; Figure 1.12). In the case of a positive nonlinear refractive index, an inverse picture will be observed: first, a minimum followed by a maximum. The amplitude of the peak indicates the magnitude of the refractive index (Sheik-Bahae et al. 1990).

Photothermal *z*-scan technique is complementary to photothermal lens spectrometry and is implemented in a similar hardware configuration and described by similar fundamental dependences (Sheik-Bahae et al. 1990; Mian, McGee, and Melikechi 2002). The wide possibilities of the *z*-scan technique make it possible even to proceed to the study of the thermal diffusivity in samples and to determine the Kerr coefficients in liquids (Alves, Bourdon, and Neto 2003, 2005).

Experiments on the determination of nonlinear optical parameters caused by electronic effects are carried out using continuous lasers (Gupte et al. 2001; Mian, McGee, and Melikechi 2002; Pilla et al. 2002a), as well as pulsed, picosecond (Sinha, Ray, and Dasgupta 2000; Pilla et al. 2002b), or femtosecond (Terazima 1995; Mian, McGee, and Melikechi 2002) lasers. Studies of nonlinear properties of reflection and absorption are carried out in glasses (Lima et al. 2001a; Imangholi, Hasselbeck, and Sheik-Bahae 2003; Jacinto et al. 2006), solutions of organic dyes and ionic liquids (Castillo, Sanchezmondragon, and Stepanov 1995; Brochard, GrolierMazza, and Cabanel 1997; Lima et al. 2001b; Alves, Bourdon, and Neto 2005), solid materials doped with ions (Catunda et al. 1997; Andrade et al. 1998, 1999, 2000; Gupte et al. 2001), and polymers (Falconieri et al. 2001; Ganeev et al. 2003).

In contrast to photothermal lens spectrometry, in *z*-scan techniques, the sample moves along the axis of propagation of the excitation beam relative to the position of the beam waist. This experiment can be carried out both in single-beam (Sheik-Bahae et al. 1990) and in double-beam (Terazima 1995) modalities while measuring a change in the irradiance of either the excitation or probe beam, respectively.

When making minimum changes to the configuration of the method by removing the pinhole (Figure 1.12), the nonlinearity of the sample absorption is measured. In these conditions, the whole beam is measured; therefore, its divergence is insignificant, and the irradiance of the transmitted radiation is affected by the radiation density in the sample, which changes as it moves relative to the focal point (Sheik-Bahae et al. 1990; Kozich et al. 1994).

Theoretical basics of the *z*-scan technique, the role of the formation of the photothermal lens element in samples, and approaches to the interpretation of experimental data are described in several publications (Bialkowski 1998; Falconieri 1999; Mian, McGee, and Melikechi 2002; Alves, Bourdon, and Neto 2003; Goswami 2006) including numerical methods for describing the effect (Kovsh, Hagan, and Van Stryland 1999). Mian, McGee, and Melikechi (2002) have shown that the role of the photothermal lens element formed in a sample is large even for femtosecond laser sources: a gradual accumulation of energy in the case of a small interval between pulses forms a photothermal lens element, distorting the influence on the probe beam of the nonlinear properties of the sample. Jacinto et al. (2006) made an excellent review on the technique.

1.5.5 Photothermal Interferometry

Shortly after the discovery of the photothermal lens effect, researchers found that the photothermal-induced refractive index change could be measured by more direct means. McLean, Sica, and Glass (1968) and Longaker and Litvak (1969) recognized that optical absorption resulting in sample heating and subsequent changes in refractive index would cause a phase shift in light passing through the heated region. The optical phase shift can be detected with an interferometer. The method of using optical interferometry to measure refractive index changes was not in itself new, but using an excitation laser to heat the sample while monitoring the refractive index change was. Most photothermal interferometry apparatuses are based on laser excitation sources. Stone (1972, 1973) showed that both coherent and wideband incoherent sources could be used. Stone used the modified Jamin interferometer apparatus shown in Figure 1.13 to obtain the absorption spectrum of chlorobenzene shown in Figure 1.14. Using this apparatus, 2–3 mW of excitation source power could be used to measure an absorption coefficient of about 2×10^{-5} cm^{-1}.

The conventional approach to measuring small absorption coefficients is to increase the optical path length. The data in Figure 1.15 compares results obtained using long path length transmission spectrophotometry to those of the photothermal interferometer. Transmission losses may be due to reflection, scattering, and absorption. The finite transmission losses seen in the bromobenzene spectrum are not necessarily due to optical absorption. On the other hand, the photothermal interferometer responds only to absorption. The resulting spectrum is technically an excitation spectrum since the heat is generated by optical absorption of the excitation light.

An almost astonishing feature of the interferometric method is its sensitivity. Davis and Petuchowski (1981) have measured absorption coefficient detection limits as low as 10^{-10} cm^{-1} for gaseous samples in windowless absorption cells using chopped IR excitation lasers at irradiances of 2.5 mW m^{-2}. Other sensitive interferometric methods for measuring

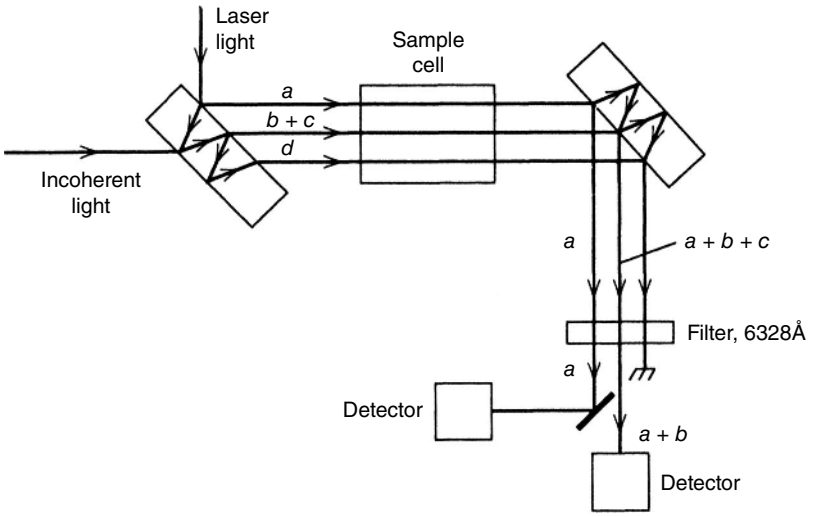

Figure 1.13 Modified Jamin interferometer apparatus used by Stone (1973). Incoherent light from a xenon arc is collimated and filtered by a series of band-pass filters before passage through the center of the sample cell along *c*. Helium–neon laser light detects the optical phase shift. The laser light is split by the optical flat and passes through a reference path *a* and a probe path *b*. The two laser beams are combined at the second optical flat. One detector monitors the power of the reference beam, and the other the power in the interfering beams $a + b$. A phase shift in the two interfering beams results in a power change at the signal detector. Phase shifts are found from the ratio of the signal to reference powers. Source: Reprinted (adapted) with permission from Whinnery (1974). Copyright 1974 American Chemical Society.

Figure 1.14 Data obtained for chlorobenzene using the photothermal interferometer of Figure 1.13 (solid) and that of bromobenzene in a glass capillary (broken line) obtained with a transmission spectrophotometer. The structured absorption features are C–H stretch vibrational overtones. Source: Reprinted (adapted) with permission from Whinnery (1974). Copyright 1974 American Chemical Society.

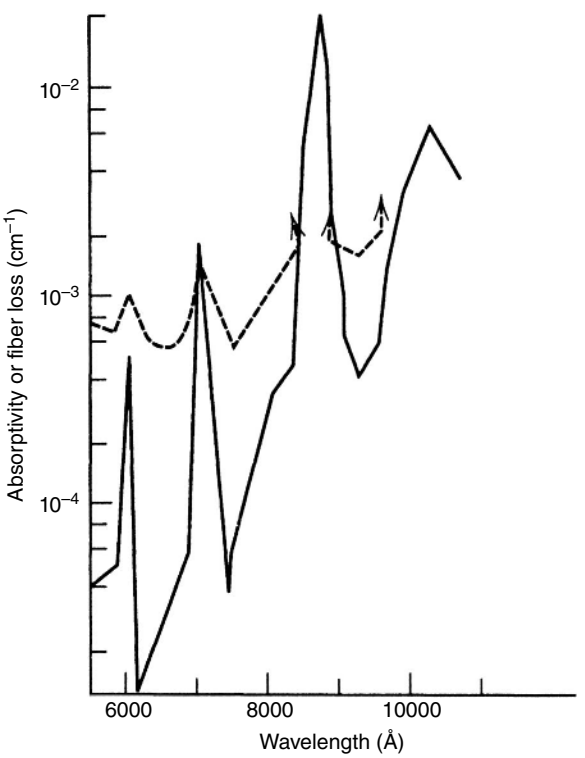

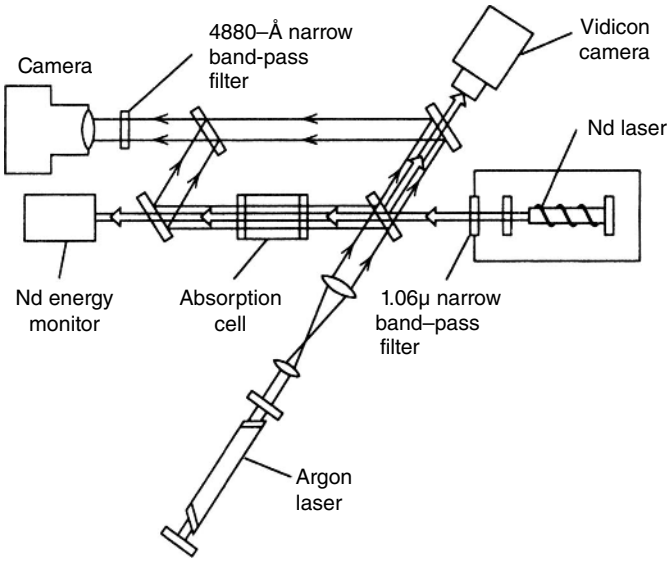

Figure 1.15 Interferometer used by Longaker and Litvak (1969) to obtain images of the density perturbation in gas and liquid samples. The pulsed Nd laser is used to excite the sample, and the continuous Ar^+ laser is used to probe the refractive index changes. The camera records the fringe shift of the Ar^+ laser beam. Source: Reprinted from Longaker and Litvak (1969) with the permission of AIP Publishing.

the photothermal effect are discussed by Friedrich (1983), and Dovichi (1987) has reviewed the applications to chemical analysis.

The interferometric studies of Longaker and Litvak (1969) used cameras to obtain images of phase shift patterns resulting from the refractive index perturbation produced by pulsed Nd–glass laser sample excitation. This classic and innovative work revealed a wealth of information regarding photothermal effects. The apparatus used for these studies is shown in Figure 1.15.

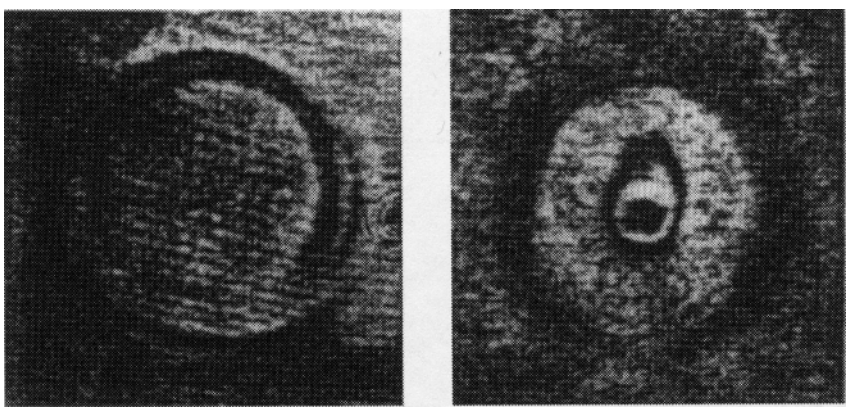

Figure 1.16 Image data obtained with the apparatus illustrated in Figure 1.15. The picture on the left is that of a 5 cm sample of nonabsorbing liquid CS_2. No thermal perturbation is observed, and the fringe shift is due only to the acoustic wave generated by electrostriction. The image on the right is for a weakly absorbing sample and has both a thermal perturbation (in the center) and an acoustic wave component (the dark ring). Source: Reprinted from Longaker and Litvak (1969) with the permission of AIP Publishing.

The photographic camera was used to obtain pictures of the fringe patterns for visual analysis, and the vidicon camera was used to obtain quantitative information for critical evaluation of the data. Photographic images shown in Figure 1.16 reveal some of effects they observed. For absorbing samples, the refractive index perturbation had two components with different space and time behaviors. A long-lived transient was observed near the region excited by the pulsed laser. This component was the thermal perturbation produced by the photothermal effect.

The phase shift, $\delta\varphi$ (rad), produced from the thermal component is related to the density change through

$$\delta\varphi = \frac{2\pi l}{\lambda}\left(\frac{dn}{d\rho}\right)\delta\rho \tag{1.14}$$

where λ is the wavelength of the laser used to measure the refractive index change. The theory developed by Longaker and Litvak predicts that for weakly absorbing samples with rapid excitation and excited state relaxation times, the on-axis time-dependent density change for pulsed radiation is

$$\delta\rho(t) \propto \frac{2\beta\alpha Q}{\pi w^2 C_P}\left(e^{-t^2/\tau_a^2} - 1\right) \tag{1.15}$$

for times much shorter than t_c. Thus the signal risetime is limited by the same acoustic relaxation time that limits the signal magnitude in photoacoustic spectroscopy. The spatial density change could be quantitatively determined by counting interference fringes. Videocon camera data were analyzed in terms of the thermal-induced phase shifts and the focal length of the photothermal lens resulting from the thermal perturbation. This later data was found to agree with the theory developed by Gordon et al. to describe the photothermal lens.

In addition to the thermal component, a short-lived transient component was found. This component propagated away from the heated region as a wave. This was identified as an acoustic pressure wave. Referring to the ammonia gas data in Figure 1.16 (image on the right), the thermal perturbation can be seen at the center, and the dark ring around the central perturbation is due to the propagating pressure or acoustic wave. The acoustic wave is produced by the rapidly expanding sample heated by the pulsed laser. The ammonia gas absorbs energy from the pulsed excitation source. Excited state ammonia rapidly relaxes, thereby increasing the temperature of the sample. The heated sample then expands to produce an acoustic compression wave. The compression wave propagates out away from the excited region. The compression increases the density of the gas, thereby causing an increase in the refractive index. Thus the acoustic wave also results in a photothermal signal. Although the acoustic wave carries away some of the energy, most of the thermal energy remains in the region local to the excitation laser irradiation (Bialkowski 1988). Although Longaker and Litvak were not the first to observe this effect, their pictorial observations clearly demonstrate the principles of photothermal and photoacoustic spectroscopies and showed the connection between the two.

Photoacoustic wave generation by the photothermal effect is only one of several mechanisms for acoustic wave generation. Figure 1.16 also shows data obtained for CS_2, a nonabsorbing, highly polarizable liquid. The CS_2 data illustrates acoustic waves created without a photothermal perturbation. The acoustic waves are generated by an effect called electrostriction wherein polarizable media are compressed by the electric field of the optical radiation. Electrostriction has not, to date, been observed using photothermal spectroscopy methods.

To implement the advantages of the photothermal interferometric method in chemistry, compact schematics of a dual-beam polarization interferometer are later proposed by Novikov, Luk'yanov, and coworkers (Luk'yanov 2000; Luk'yanov and Novikov 2000; Luk'yanov et al.

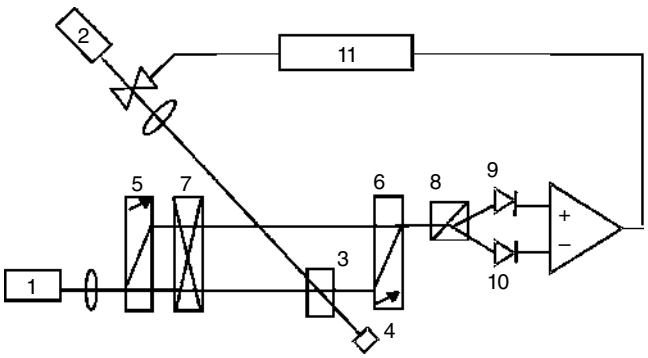

Figure 1.17 Block diagram of photothermal polarization interferometer (see text for the details); *1*, probe laser (680 nm, 10 mW); *2*, excitation laser (25 mW, 532 nm; Laser Compact, Russia); *3*, Z-geometry cell; *4*, power meter for the excitation laser; *5* and *6*, $CaCO_3$ Savart plates; *7*, a rotator on 90°; *8*, a Wollaston prism; *9* and *10*, photodiodes; *11*, lock-in amplifier. Source: Luk'yanov et al. (2003). Reproduced with permission from American Institute of Physics.

2003). Here, in a Jamin–Lebedev interferometer, the optical phase shift between two probe beams is transformed into a change in the ellipticity or asymmetry of the light polarization at the output of the instrument (Figure 1.17). A small-sized frequency-doubled Nd:YAG laser is used as an excitation source. The modulation frequency of the excitation beam is determined by a built-in generator in the range from 30 to 100 Hz. A semiconductor laser serves as a probe. The most relevant feature of the interferometer is a $\pi/2$ difference between its lever arms. The interferometer has two working modes: refractometric and photothermal. In both modes, the initial phase is tuned by a feedback system that keeps the interferometer at this working point.

In the refractometric mode, the excitation beam is turned off, and slow nonperiodic changes in the refractive index of flow-through liquid are measured (lock-in time constant is 0.3 second). The corresponding electrical signal caused by a change in the refractive index due to the flowing liquid composition is formed in the feedback system as an error signal.

In the photothermal mode, in the presence of an absorbing substance in the analyte cell, the temperature and refraction index of the eluent start to oscillate at the modulation frequency because of the photothermal effect. Thus, an additional alternating phase difference between interferometer arms appears, and the polarization state at the output of the second Savart plate (*6*) is modulated (see Figure 1.18). The amplitude of the modulation is analyzed by a Wollaston prism (*8*) and is recorded by photodiodes (*9*) and (*10*). The change in the ellipticity is readily measured by a conventional built-in lock-in amplifier (*11*) coupled to these photodiodes.

A similar schematic was built for the assessment of surface and volume absorption of optical elements and their coatings and similar complex transparent samples (Brazhnik, Novikov, and Pushkin 1990; Brazhnik and Novikov 1991b).

The signal in the photothermal mode of this interferometer as a difference in the phase upon the periodical excitation of the photothermal effect is calculated as

$$\Delta\varphi = \frac{4}{\lambda}\frac{\Phi_0}{w^2}\frac{\partial n}{\partial T}\frac{\alpha l}{\rho C_P \omega} \tag{1.16}$$

Here, ω is the angular frequency of the excitation beam. The feedback system keeping the working point provides a significant increase in the performance parameters of such an interferometric schematic. The instrument provides the linear dynamic range of absorbances of 10^5 and

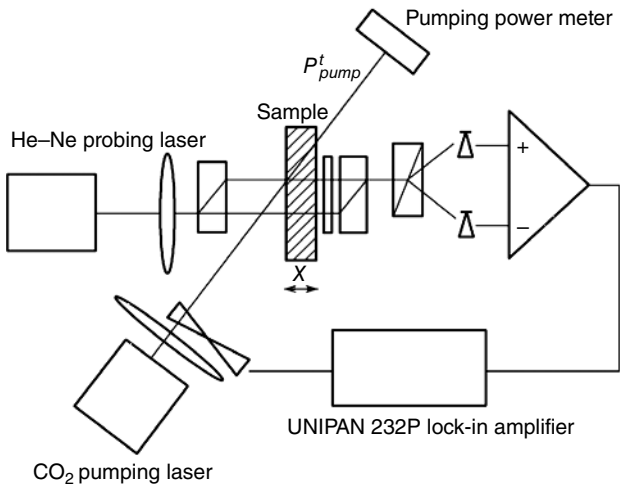

Figure 1.18 The scheme of the experimental setup. HeNe laser model LGN-302; CO_2 laser pump model LH-74, medium power 1 W; lock-in amplifier model UNIPAN, 232P. The achieved sensitivity of optical absorption coefficient is no worse than 10^{-5} cm^{-1} for bulk absorption and 10^{-6} for surface absorption, with a measurement error of 30%. Source: Copyright Luk'yanov and Pogorelko (2002). Reproduced with permission of Springer–Nature.

enhanced measurement precision compared with transmisssion spectrophotometry. The photothermal interferometer is characterized by the minimum optical absorption coefficient α_{min} of 2×10^{-10} cm^{-1} and an increase in sensitivity compared with transmission measurements of 10^4 (Luk'yanov et al. 1999, 2003; Luk'yanov and Novikov 2000; Luk'yanov and Pogorelko 2002).

Such interferometers are simple to adjust, very stable in functioning, and resistant to environmental noises. For analytical chemistry, it is important that the total noise of such a photothermal interferometer as a detector in liquid chromatography or flow analysis is at least an order lower than the noises from the majority of HPLC pumps (Weston and Brown 1997). Diameters of probe beams in the detector cell are 100 μm, which provide rather low signal generation volumes. The region of the interaction between the probe and excitation beams in the cell channel is 1 cm in length (Brazhnik and Novikov 1991a; Morozov, Novikov, and Raevskii 1992). The size of interferometers is rather compact (20 × 5 × 20 cm).

1.5.6 Two-Beam Photothermal Lens Spectroscopy

The two-laser photothermal lens apparatus was used before the extracavity single-laser method was found. Grabiner, Siebert, and Flynn (1972) used a helium–neon laser to probe the photothermal lens produced by a pulsed IR laser. They used this two-laser photothermal lens apparatus to determine the vibrational relaxation rate constants for methyl chloride and methyl fluoride. Later, Siebert, Grabiner, and Flynn (1974) used the technique to study relaxation of vibrationally excited CD_4, SO_2, and OCS. Of interest was the risetime of the photothermal lens signal. The risetimes were measured as a function of added gas pressure, and the vibrational relaxation rate constants were deduced from these measurements. The technique was found to be quite satisfactory for relaxation times that were greater than the acoustic-limited risetimes. The vibrational relaxation rate constants compared well with those obtained using other methods. Although not exploited in this work, Grabiner et al. and Siebert et al. showed that by using this photothermal lens method, IR absorption could be measured using visible detectors. This would later be used to the advantage of short path length IR absorption studies.

Long, Swofford, and Albrecht (1976) used the two-laser photothermal lens apparatus shown in Figure 1.19 to measure absorption spectra due to vibrational overtones in pure solvents. A repetitively chopped continuous dye laser was used to form the photothermal lens in the

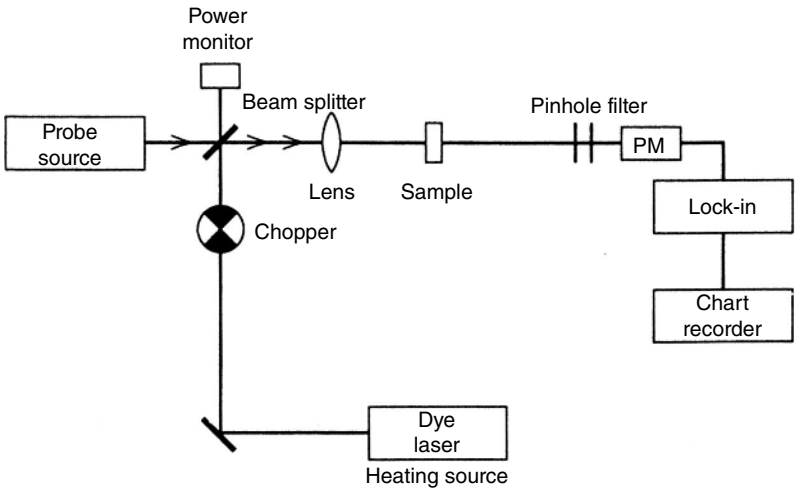

Figure 1.19 A dual-beam photothermal lens spectrometer. The dye laser excites the sample, and the probe source monitors the resulting refractive index change through the photothermal lens effect. The diverging probe beam passes through a pinhole spatial filter to develop the signal. The wavelength filter rejects the excitation wavelength. The chopped signal is processed with a lock-in amplifier to improve the signal-to-noise ratio. The dye laser can be scanned to obtain photothermal excitation spectra. Source: Reprinted from Swofford and Morrell (1978) with the permission of AIP Publishing.

sample, and a continuous helium–neon laser probed the resulting lens element. The equations that describe the temperature change and focal length of the photothermal lens are the same as those given above. However, several advantages to using separate excitation and probe light sources in photothermal lens spectroscopy can be realized in this configuration: (i) The dye laser can be scanned to produce excitation spectra of the sample without having to account for photodetector wavelength response. (ii) The excitation source can be focused directly into the sample. This increases the irradiance and the resulting photothermal lens signal by decreasing the beam waist radius in the sample. (iii) A lock-in amplifier can be used to decrease the bandwidth of the measurement, thereby enhancing the signal-to-noise ratio.

Twarowski and Kliger (1977a, b) developed a quantitative theory to describe the pulsed laser excited photothermal lens spectroscopy signals and applied this theory to study the two-photon absorption of benzene. This was the first derivation of the time-dependent photothermal lens given for pulsed laser excitation. Basically, a pulsed laser with an integrated irradiance $H(r,t)$ (J m^{-2}) of

$$H(r,t) = \frac{2Q}{\pi w^2} e^{-2r^2/w^2} \tag{1.17}$$

will produce a temperature change of

$$\delta T(r,t) = \frac{2\alpha Q}{\pi w^2 \rho C_P} \frac{e^{-2r^2/w^2(1+2t/t_c)}}{1+2t/t_c} \tag{1.18}$$

for a single-photon absorption process and for times greater than required for acoustic relaxation. The inverse focal length was found to be

$$\frac{1}{f(t)} = \frac{1}{n_0}\left(\frac{dn}{dT}\right)\frac{8\alpha l Q}{\pi w^4 \rho C_P}\frac{1}{(1+2t/t_c)^2} \tag{1.19}$$

The main characteristics of the pulsed laser photothermal lens spectroscopy signal are as follows: (i) the signal magnitude is greatest at zero time, just after acoustic relaxation of the sample. This allows the pulsed laser technique to be used to study excited state relaxation kinetics. (ii) The signal is inversely proportional to w^4, favoring tighter focused beams. (iii) The signal decays in a time that is inversely proportional to t^2. (iv) As with the chopped continuous excitation laser method, the pulsed laser method can use dye lasers to obtain excitation spectra, and the excitation laser can be focused into the sample cell, resulting in greater signal magnitudes. (v) The high irradiance at the focus can be high enough to induce nonlinear absorption effects. The multiphoton absorption signal is essentially the same but with the caveat that the absorbed energy is proportional to the integrated irradiance raised to the power of the number of photons absorbed. Thus the effective squared beam waist radius is decreased by a factor inversely proportional to the number of photons absorbed per transition, $w^2/p \rightarrow w^2$. This further enhances the signal magnitude and has led to the belief that photothermal lens spectroscopy is very useful for multiphoton spectroscopy.

Barker and Rothem (1982) pointed out that the simple theoretical description of the photothermal lens shown above does not yield quantitative results in the early times of the signal. They point out an apparent dilemma wherein Grabiner, Siebert, and Flynn (1972) use an acoustic wave equation to model results while Twarowski and Kliger (1977a) use a thermal diffusion equation. Barker and Rothem developed a quantitative theory for predicting the photothermal lens signal that takes into account several hydrodynamic relaxation effects. This theory predicts that all but the first of the five points given above hold but that the signal risetime is limited by the rate at which the density can change. The latter is related to the sound velocity and the radius of the excitation source (Barker and Toselli 1989).

Fang and Swofford (1983) have written an excellent overview of the theory and developments in photothermal lens spectroscopy. Dovichi (1987) has reviewed the literature and has commented on analytical applications of the technique, including absorbance detection limits of about 10^{-7}–10^{-8} cm^{-1} for liquids and gases using 10–200 mW continuous sources. Sell (1989) has collected together a number of chapters addressing many important applications of photothermal spectroscopy. Morris and Fotiou (1987) have reviewed applications to chromatography detection. Dovichi (1990) has included this technique in his review of laser-based microanalysis. Snook (1997) and Georges (1999) made detailed overviews of features and limitations of photothermal lens spectrometry in applied chemistry. Franko and Tran (1996, 2006) made detailed reviews on specific features of photothermal lens spectrometry in applied studies. Proskurnin et al. made several reviews on photothermal lens spectrometry along with other photothermal methods and hyphenation with flow separation techniques (Proskurnin and Kononets 2004; Proskurnin 2014; Proskurnin et al. 2015; Proskurnin, Bendrysheva, and Smirnova 2016). Franko (2008) made a special review of photothermal lens spectrometry in flow analysis. Liu and Franko (2016) have written a short essay about the outlooks of applied photothermal spectroscopy.

1.5.7 Photothermal Lens Microscopy

From the very beginning, the locality of photothermal spectroscopy and possible scaling down of photothermal optical schematics and apparatuses were discussed (Sepaniak and Kettler 1984; Kitamori 1999; Kenji et al. 2000; Hibara et al. 2001a; Ghaleb and Georges 2004). At present, many photothermal microscopic techniques have been introduced, and photothermal lens microscopy (thermal lens microscopy) is one of the most rapidly developed areas of photothermal spectroscopy (Liu and Franko 2014b).

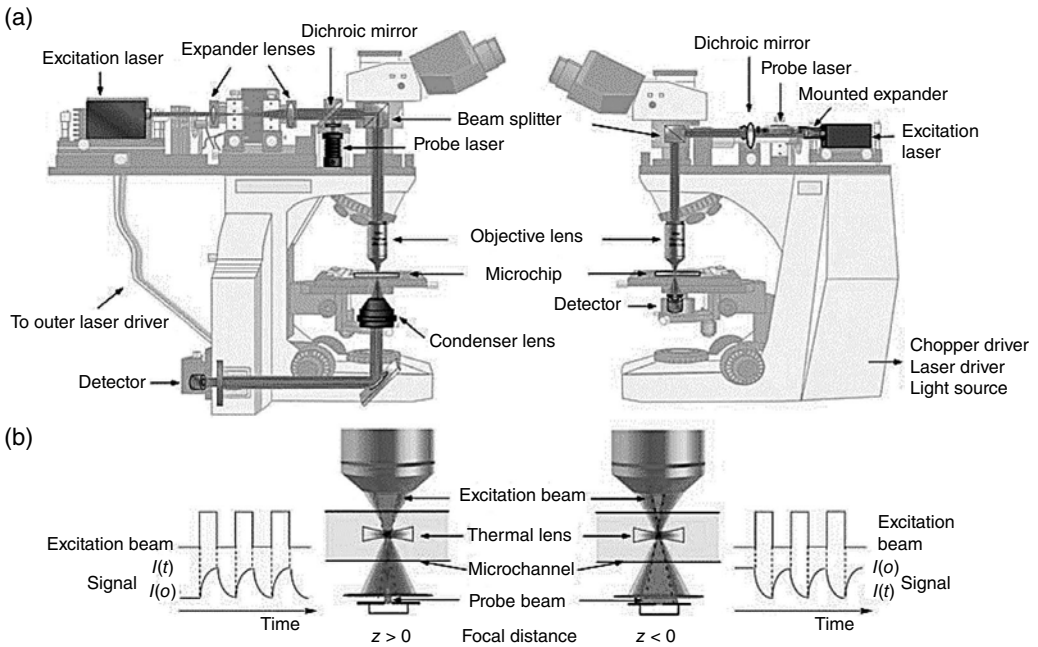

Figure 1.20 (a, b) Schematic diagram of compact thermal lens microscopes for analytical measurements in microfluidic chips. Source: Smirnova et al. (2012). Reproduced with permission of Wiley.

In this method, the spatial distributions of probe beam amplitude and phase also serve as a signal (Tokeshi, Minagawa, and Kitamori 2000; Hibara et al. 2001b; Hisamoto et al. 2001; Kitamori 2001; Ragozina et al. 2002, 2004). Although the signal formation mode, theoretical basics, and instrumentation of photothermal lens spectrometry and microscopy coincide in many respects, they are not identical (Khodakovskaya et al. 2011; Nedosekin et al. 2011, 2012a, c, 2013; Proskurnin et al. 2011; Tuchin, Tárnok, and Zharov 2011; Galanzha and Zharov 2012).

Photothermal lens microscopy was specially developed for measuring signals in a microspace; before passing through the sample, laser radiation is collected and directed by means of an optical microscope (Figure 1.20). Thus, the microscope is additionally included in the optical schematic of a photothermal lens spectrometer (Smirnova et al. 2012). The crucial difference of photothermal lens microscopy from conventional photothermal lens spectrometry consists in the configuration of laser beams in the sample.

In double-beam photothermal lens spectrometry, a cell with the sample is arranged after the waists of excitation and probe beams; under the action of the photothermal lens, the probe laser beam diverges and its irradiance decreases (Hiki et al. 2003). In photothermal lens microscopy, both beams are collected by an objective lens and focused. In the absence of objective lens aberrations, the focal positions of the excitation (the photothermal lens blooming point) and probe lasers coincide (Figure 1.20).

In this case, the appearance of a lens has no effect on the divergence of the probe laser beam. Usually, the chromatic aberration in objectives intended for observing microsamples is completely compensated because it impairs the quality of images (Hiki et al. 2003; Proskurnin et al. 2003). Standard compensated objectives are used in photothermal lens microscopy, and

the distance between beam foci is adjusted by double-lens expanders (Kitamori et al. 2004). Both beams pass through the expanders, which are used for fine-tuning the distance between beam waists and the size of beams in the sample. With the aid of dichroic mirrors, the beams are collected and coaxially directed through an objective lens of the optical microscope.

The main differences of photothermal lens microscopy from photothermal lens spectrometry can be summed as follows: (i) the position of the focus of the excitation and probe laser beams in a microchannel makes it possible to easily focus the thermal heterogeneity as a sharp image in the microscope objective/camera/detector; (ii) a decrease in the optical path length by two or three orders of magnitude leads to local photothermal effects; (iii) a decrease in the radii of laser beams in the sample makes it possible to conduct scanning in both horizontal and vertical directions; and (iv) the focusing effect due to the position of the focus of the probe beam after the focus of the excitation laser leads to an increase in the signal.

The image of the sample can be observed visually or displayed by a CCD camera through the second objective lens. The sample (a microcell or microfluidic chip) is arranged on the objective table, whose position can be adjusted in three mutually perpendicular directions. After passing through the sample and further through a collecting lens, the probe beam is separated from the excitation beam using narrowband optical and interference filters. Finally, after passing through a pinhole, the information-bearing probe beam arrives at a photodiode detector connected to a lock-in amplifier. The signal from the amplifier is transferred to an analog-to-digital/digital-to-analog converter.

Photothermal lens microscopy was developed primarily for integrated microanalysis systems (microfluidic chips) (Kitamori 1999; Kenji et al. 2000; Hibara et al. 2001a). This has led to the commercially produced photothermal instruments, namely, microscopes of the ITLM series (Institute of Microchemical Technology, Japan) used from the beginning of 2000s in a great number of relevant studies (Aota and Kitamori 2010; Mawatari et al. 2011, 2012; Shimizu, Mawatari, and Kitamori 2011; Yamamoto et al. 2011; Smirnova et al. 2012), which were specially designed for analytical applications related to microfluidic systems and beyond.

Serially produced tabletop photothermal lens microscopes show high sensitivity and good applicability range; furthermore, they are convenient and portable as detectors. At present, these instruments find ever-widening use (Hiki et al. 2003; Kitamori et al. 2004) and actively conquer the market of analytical instruments in Japan, the United States, and Europe.

Still, this direction of development of photothermal lens microscopy is not the only route. As commercially available microscopes provide a wide but still limited range of predefined sets of features, some specific applications are based on unique builds of microscopes. One of the variants was made for the hyphenation of microflow injection analysis (Liu and Franko 2014a; Liu et al. 2014; Radovanović et al. 2015). Liu, Korte, and Franko (2012) gave a theoretical description of the features of this variant of photothermal microscopy. A broadband incoherent light source was introduced into a photothermal lens microscope to improve the specificity (Liu and Franko 2012).

Another variant of photothermal lens microscopy was built especially for *in vivo* investigations (Zharov et al. 2002; Nedosekin et al. 2010). Nedosekin et al. (2012b) proposed confocal schematics of photothermal lens microscopy, providing high-resolution three-dimensional imaging of nonfluorescent molecules with scanning and time-resolved detection, with a tunable pulsed nanosecond excitation laser. By the use of dependence of photothermal lens signal of thermal properties, a resolution below the diffraction limit is claimed (Nedosekin et al. 2014).

Photothermal lens microscopy makes it possible to study the course of analytical reactions at a nanogram level and to combine it with microflow analysis and microchromatography. Its use is

also directly related to the development of microflow injection analysis, electrophoresis on microfluidic chips, and, in general, integrated microanalysis systems (microfluidic systems; see Chapter 7) (Tokeshi, Minagawa, and Kitamori 2000; Hibara et al. 2001b; Hisamoto et al. 2001; Khodakovskaya et al. 2011; Nedosekin et al. 2011).

From the beginning of 2000, efforts were focused on the development of photothermal modalities capable of measuring single submicrometer particles. One of the first to be proposed was *photothermal interference contrast*. In this method, the interferometric detection technique – difference interference contrast – is used for the detection of the strength of a photothermal effect caused by single nano-sized particles with the separation of the probe beam into main and reference beams (Boyer et al. 2002; Cognet et al. 2003). Later, a related method, *photothermal heterodyne spectroscopy* (more correct, microspectroscopy), which is technically simpler than photothermal interference contrast, was developed. The photothermal effect, which appears upon the absorption of an excitation beam by a particle, causes the scattering of the probe beam, which can be detected as a fluctuation of the probe irradiance due to the interference of the initial beam and scattered radiation (Berciaud et al. 2004, 2006; Papernov et al. 2011). This method has higher sensitivity than photothermal interference contrast and is capable of detecting changes in the environment of heated single (large) molecules like DNA (Blab et al. 2006). The principle of photothermal heterodyne measurements can be used as imaging (Berciaud et al. 2006) and spectroscopy for absorption spectra of single nano-sized particles (Berciaud et al. 2007; Berciaud, Cognet, and Lounis 2008).

Raduenz et al. (2009) developed a more advanced technique based on photothermal heterodyne spectroscopy, called *photothermal correlation spectroscopy* (once again, as this modality is based on the use of a microscopic technique, a more correct name is microspectroscopy). It is based on building an autocorrelation function G for the time-resolved photothermal signal S:

$$G(\tau) = \frac{\langle S(t)S(t+\tau)\rangle}{\langle S(t)\rangle^2} \tag{1.20}$$

which, provided that the characteristic times of the instrumentation (like the lock-in detection time constant) are known, can be used for acquiring the characteristic time τ of the heat-releasing processes during the photothermal experiment. As the photothermal processes for nanoparticle solutions depend on the thermal and optical properties of nanoparticles and their motion velocity, photothermal correlation spectroscopy can be used for detecting, monitoring, and characterizing such objects.

Selmke, Braun, and Cichos (2012a,b) reported that any single absorber particle acts like an analog of the macro-photothermal lens, a nano-lens, which can be detected using a scattering pattern of the probe radiation from a "halo" of the thermally induced field from a heated particle. The combination of the nano-lens concept, mode mismatched excitation–probe alignment, and correlation spectroscopy allowed Selmke et al. (2013) to develop a very promising microscopic analog of the differential photothermal technique, which is called twin-focus photothermal correlation spectroscopy. This technique is based on the detection of two spatially separated volumes of the sample corresponding to beam configurations (like for the photothermal z-scan technique) and building two autocorrelation functions for each of the volumes separately. Similarly to differential techniques described in Chapter 6 with a large dynamic reserve (see Section 6.2.1), this technique renders very sensitive and precise measurements. It provides a tool for precise measurements of slow motion along the beam propagation axis or very slight heterogeneities in sub-diffraction-limited length scales in the sample due to the amplification of differences in the photothermal responses in both volumes, one of which can act as a reference.

1.5.8 Photothermal Deflection, Refraction, and Diffraction

The mirage is a common and well-understood example of the photothermal effect. However, the analytical method based on this principle, photothermal deflection spectroscopy, was somehow overlooked until Boccara, Fournier, and Badoz (1979) demonstrated probe laser beam deflection in 1979. The method was applied to surface analysis. A typical experimental setup for photothermal deflection analysis of surfaces is shown in Figure 1.21c. Like the indirect photoacoustic spectroscopy method, this method may be used to examine optical absorptions at or near the surface of solid samples. The sample absorbs optical radiation and heats the gas or liquid above the surface. The heated gas acts like a prism and deflects the probe laser incident tangent to the

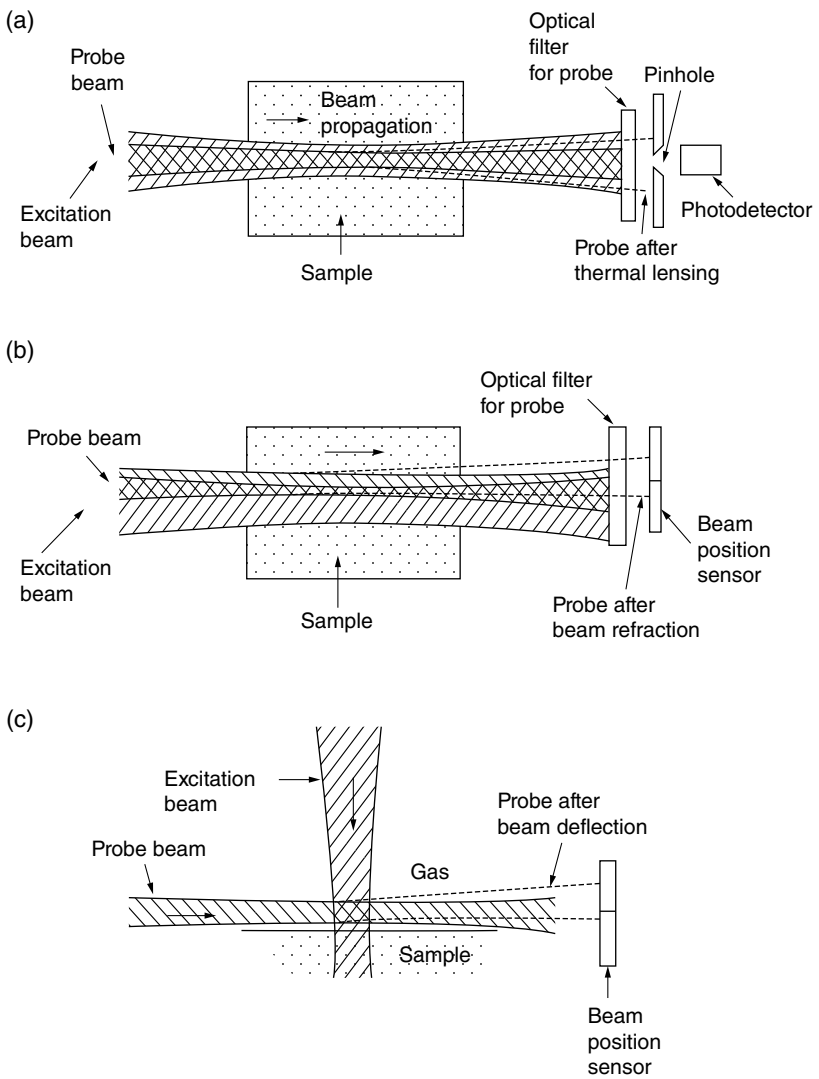

Figure 1.21 Various excitation and probe beam geometries used in photothermal spectroscopy. (a) Thermal lensing. (b) Parallel PT probe beam refraction. (c) Perpendicular PT probe beam refraction. Source: Reprinted figure with permission from Tam (1986). Copyright 1986 by the American Physical Society.

surface. Probe laser beam deflection is monitored with a position sensing detector. The apparatus is very easy to set up and can produce very sensitive measurements of surface absorption.

The theory for describing the photothermal deflection signal has been worked out for both chopped and pulsed excitation sources. This theory is more complicated than those describing homogeneous fluids because the thermal conduction in the solid and the fluid must both be accounted for. The temperature change that occurs upon pulsed irradiation of a surface with an adsorbed absorbing species is

$$\delta T_f(x,t) = \frac{\kappa_S H}{\rho_s C_{P,s} D_{T,s}^{1/2} + \rho_f C_{P,f} D_{T,f}^{1/2}} \frac{1}{(4\pi t)^{1/2}} e^{-x^2/4D_{T,f}t} \tag{1.21}$$

where the x direction is normal to the surface, κ_S is the unitless surface absorption coefficient, and D_T and ρC_P are the thermal diffusivities and heat capacities of the solid (s) and fluid coupling medium (f), respectively. The deflection angle of a probe being refracted by the temperature gradient produced by the heated surface is

$$\varphi(x,t) = -\left(\frac{dn}{dT}\right) \frac{\kappa_S H}{\rho_s C_{P,s} D_{T,s}^{1/2} + \rho_f C_{P,f} D_{T,f}^{1/2}} \frac{x}{4D_{T,f}\sqrt{\pi} t^{3/2}} e^{-x^2/4D_{T,f}t} \tag{1.22}$$

The deflection angle is monitored using a position sensing detector that is placed a short distance from the surface. A change in angle at the sample results in a displacement of the probe laser spot on the detector. For small angles, the linear displacement of the probe laser beam spot is directly proportional to the deflection angle. The above equation shows that the magnitude of the signal will be a function of the offset, x, of the probe laser beam from the surface. There is an optimum offset for maximum signal. This optimum offset is a function of time. The time is that required for the temperature change to diffuse to the region probed by the laser. The temperature diffusion process is often called the thermal wave. This equation also shows that at a particular offset, the time-dependent deflection signal will rise and then fall with time. The time to the maximum is $t_{max} = x^2/6D_{T,f}$. So the time to the maximum signal and the magnitude of the maximum signal are both functions of the displacement of the probe laser beam relative to the surface. This distance is difficult to measure and so photothermal deflection cannot be used to measure absolute absorption coefficients.

One application of this technique caught on rapidly. It was apparent that photothermal deflection could be used for topographic and thermal characterization of samples. The signal magnitude depends on the surface topography, surface absorption coefficient, the thermal properties of the fluid, and the thermal properties of the solid. All other parameters being equal, the signal dependence on the surface to probe laser beam offset allows the surface topography to be measured. For relatively flat surfaces, signal dependence on the solid's thermodynamic parameters allows a *thermal image* of the solid to be obtained (Murphy and Aamodt 1980, 1981). A solid with a constant surface absorption or an optically dense solid will result in a signal that is inversely proportional to the solid's thermal conductivity. An example of a thermal imaging apparatus is shown in Figure 1.22. When the solid sample is raster scanned under a focused excitation laser source, the photothermal deflection signal magnitude will be inversely proportional to the solid's thermal parameters. This thermal imaging technique has been used to determine sample thickness, inclusions in metals (McDonald 1986), inspect coatings (Busse 1989), and imaging boundaries at crystal domains (Murphy, Maclachlan, and Aamodt 1986). The thermal image shown in Figure 1.23 is of aluminum metal. The lighter regions are thought to be due to subsurface inclusions in the metal. Several applications of photothermal deflection spectroscopy have been discussed in the chapter by Fournier and Boccara (1988).

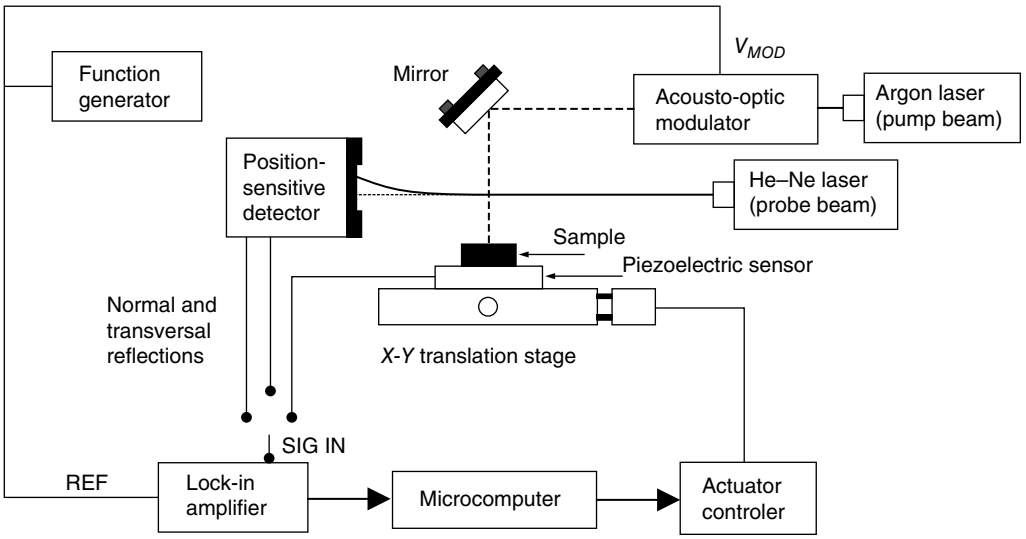

Figure 1.22 Photothermal deflection apparatus used to measure the photothermal image of a surface. The magnitude and phase of the photothermal deflection signal are measured at each position of sample excitation. The sample is raster scanned using the *x–y* translational stage. The microcomputer records the data and performs image analysis. Source: Adapted from Murphy, Maclachlan, and Aamodt 1986).

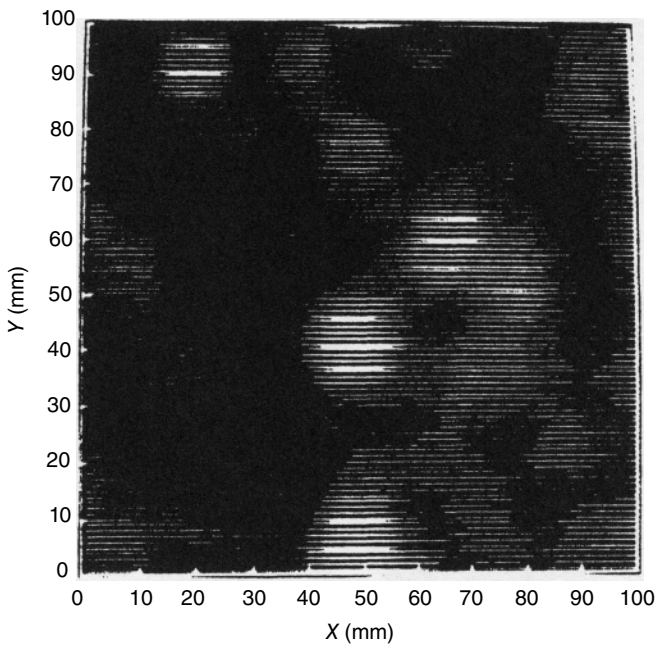

Figure 1.23 A photothermal deflection image of an aluminum surface. Source: Adapted from McDonald (1986). Reproduced with permission from Canadian Science Publishing.

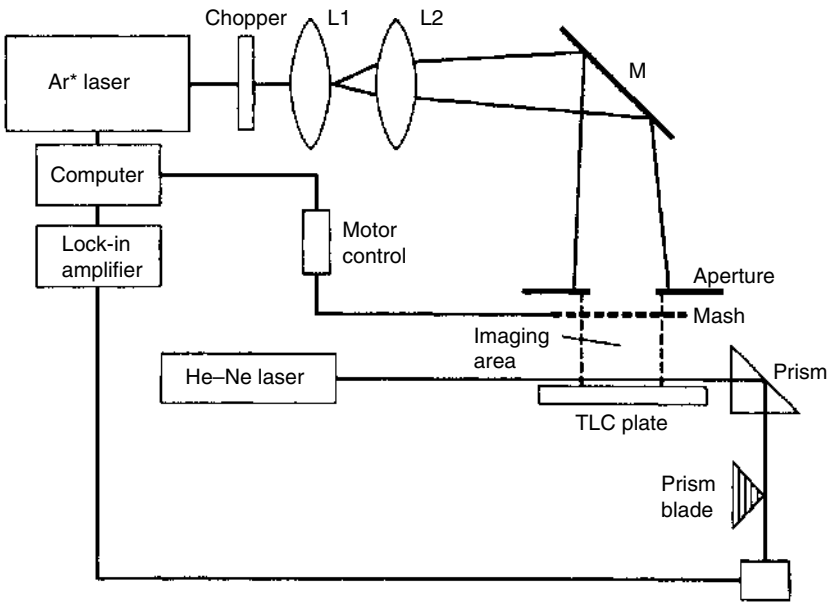

Figure 1.24 One-dimensional imaging apparatus developed for plate chromatography based on a time-multiplexed Hadamard encoded mask. Each position of the mask results in a unique surface excitation pattern. A photothermal deflection signal is recorded for each position of the mask, and the resulting data set is transformed. The transformed data yields the absorption image of the thin-layer chromatography plate. Source: Reprinted with permission from Fotiou and Morris (1987). Copyright 1987 American Chemical Society.

A useful extension of this technique is to irradiate the entire surface with a series of patterns instead of scanning the excitation and probe lasers across the surface. Fotiou and Morris (1986) use a moving Hadamard encoded mask to analyze the spatial distribution of absorption on stationary thin-layer chromatography plates. This method is more fully described in Morris and Fotiou (1987). A typical apparatus is shown in Figure 1.24. This apparatus was used to measure band positions and absorptions on dyed plates. Imaging thus far has been one-dimensional, but there is no apparent reason why two-dimensional images could not be obtained.

Boccara et al. (1980) and Jackson et al. (1981) extended the photothermal deflection method to include optically transmitting gas and liquid analysis. In these experiments the excitation and probe lasers propagate collinearly through the sample cell. In this case the pulsed laser-induced temperature change results in the deflection of a collinear probe beam:

$$\varphi(r,t) = -\left(\frac{dn}{dT}\right)\frac{8r\alpha lQ}{\pi w^4 \rho C_P} e^{-2r^2/w^2(1+2t/t_c)} \tag{1.23}$$

There is a subtle distinction between the photothermal methods used for surface and transparent sample analysis. For surface analysis, the probe laser is used to detect a refractive index gradient formed in the media above the surface. In transparent samples, the refractive index is changed within the sample itself. Thus the deflection angle signal is essentially the same as the pulsed laser photothermal lens inverse focal length. In fact, the signal strengths observed are about the same (Jackson et al. 1981). This method is very similar to photothermal lens spectroscopy. The similarity between the photothermal lens method and the beam deflection technique has been noticed by many authors, for example, see Tam (1983, 1986, 1989) and Dovichi (1987). Photothermal lens and photothermal deflection methods both rely on the generation of a

refractive index gradient in the sample itself. Collectively, they have become known as refractive index gradient detection or photothermal refraction spectroscopy methods (Tam 1986; Zharov and Letokhov 1986). The different geometries for sample excitation and monitoring of the photothermal response are shown in Figure 1.21.

The main advantage of photothermal deflection spectroscopy is its versatility. The same method can be used for solid-, surface, liquid-, and gas-phase analysis. Excitation sources can be either pulsed or chopped continuous. The absorption coefficient detection limits for these methods are about the same as those of the two-laser photothermal lens method. Fournier et al. (1980) demonstrated absorption coefficient detection limits of 10^{-7} cm^{-1} for gas-phase samples in a windowless flow cell using a 1 W modulated IR carbon dioxide excitation laser. Long and Bialkowski (1985) used a 10 mJ pulsed IR laser to obtain gas-phase absorption coefficient detection limits equivalent to 10^{-8} cm^{-1}. Bialkowski and He (1988) later used an etalon to amplify the deflection angle signal and found a 100-fold signal-to-noise ratio improvement, or approximately 10^{-10} cm^{-1} detection limit for a 10 mJ pulse. Jackson et al. (1981) demonstrated 10^{-6} cm^{-1} absorption coefficient detection of benzene in CCl_4 using a 1 mJ pulsed dye laser. The solvent itself had an absorption coefficient of 10^{-6} cm^{-1}, and absorption due to the benzene analyte was found by scanning the wavelength of the pulsed pump laser. The estimated limit of absorption coefficient detection was 10^{-7} cm^{-1}. Dovichi (1987) pointed out that the photothermal refraction methods are advantageous when there is a significant signal due to sample cell window absorbance. Since the excitation and probe lasers do not have to pass into the sample at the same spot, photothermal perturbations due to the window can be ignored. There have been several reviews on probe beam deflection techniques. These reviews are often compiled along with those for photoacoustic spectroscopy. The reviews by Tam (1983, 1986, 1989), Murphy, Maclachlan, and Aamodt (1986), Dovichi (1987), and Fournier and Boccara (1988) all cover aspects of this method. The books edited by Mandelis (1987) and Hess (1989a,b) have chapters devoted to this method.

Another method based on the generation of refractive index changes within the sample is photothermal diffraction spectroscopy. Laser-induced gratings have been known for quite some time (Eichler, Günter, and Pohl 1986) and are the basis of optical holography (Collier, Burckhardt, and Lin 1971). However, the first analytical application was by Pelletier, Thornsheim, and Harris (1982), who demonstrated that a refractive index grating could be formed in a weakly absorbing sample by interfering two beams from a single excitation laser within the sample. The apparatus is shown in Figure 1.25. The grating diffracts a probe laser beam at a specific angle that satisfies the Bragg condition.

For pulsed laser excitation, the diffracted probe beam power is (Pelletier and Harris 1983)

$$\frac{\Phi_+}{\Phi_0} = \frac{2\pi}{\sqrt{3}} \left[\left(\frac{dn}{dT} \right)_p \frac{Q\alpha}{\rho C_P w \lambda \sin 2\theta} \right]^2 \tag{1.24}$$

Here Φ_+ is the diffracted and Φ_0 is the incident probe laser power, Q is the total (combined) pulse energy, λ is the wavelength of the probe laser, and 2θ is the angle between the two pulsed pump laser beams. The diffraction signal is proportional to $(\alpha Q)^2$, thus apparently limiting the sensitivity at low concentrations. However, unlike IR emission, the background is very small. The background noise limitation is essentially the same as that of laser-excited fluorescence spectroscopy. Current absorbance detection limits are about 10^{-6} cm^{-1}. Although not exploited to any great extent, this method has potential for trace analysis. The main advantage of this technique is apparently in the relatively simple data that result when the sample undergoes nonlinear absorption. In this case the distorted grating formed by nonlinear absorption can be decomposed by Fourier analysis into a series of orthogonal gratings, each with a different spatial period.

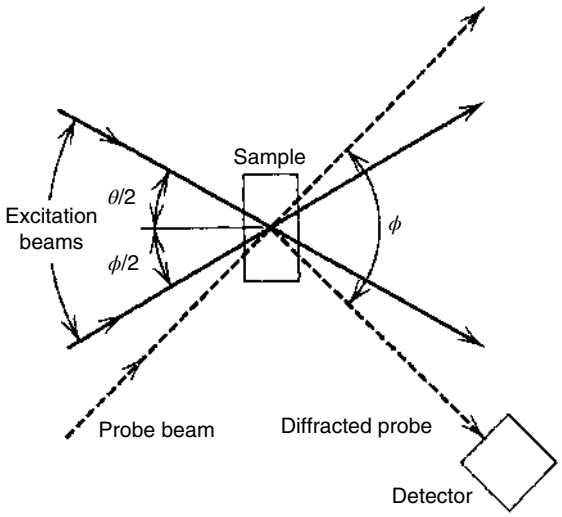

Figure 1.25 A schematic of an apparatus used for photothermal diffraction. The two excitation beams are mutually coherent, arising from the same laser excitation source. Interference of the two beams produced a periodic irradiance and subsequently a periodic refractive index perturbation, or phase grating, in a weakly absorbing sample. The phase grating is probed with a second probe laser. Source: Reprinted (adapted) with permission from Pelletier, Thornsheim, and Harris (1982). Copyright 1982 American Chemical Society.

Each grating then produces a different diffraction angle. The type of nonlinear absorption can be determined by analysis of the magnitude and irradiance dependence of the probe laser at each diffraction angle. The connection between photothermal lens, photothermal refraction, and photothermal diffraction spectroscopies has been given by Harris (1986), and the principles and applications of the photothermal diffraction method have been reviewed by Zhu, McGraw, and Harris (1992).

Weimer and Dovichi (1988) reported on a pulsed laser excited photothermal lens apparatus that utilized a photodiode array to simultaneously detect the spatially dependent photothermal lens elements produced as the excitation beam traverses a relatively high absorbance sample. A pulsed nitrogen pumped dye laser was focused through a 1 cm length cuvette. The probe laser was defocused to a size that would probe the length of the sample cell and directed through the sample at right angles to the excitation beam. After passing through the sample, the probe beam was focused onto the photodiode array with a cylindrical lens. The cylindrical lens presumably also served as the spatial filter in this case. Each element of the photodiode array corresponded to a different position within the sample. The photodiode array was read out with each pulse of the excitation laser and averaged to improve the signal-to-noise ratio. The probe laser irradiance recorded by each element of the array corresponded to a different position along the length of the sample. Examined in total, the photodiode array signal showed the effect of pump laser beam attenuation as it traversed the sample. The spatially dependent attenuation of the excitation source was observed as a decrease in the spatially dependent photothermal lens signal. Absorption of the excitation source was obtained by simply observing the spatially dependent photothermal lens strength.

Another photothermal deflection spectroscopy variant was proposed, *photothermal cantilever deflection spectroscopy*, designed to detect traces of substances in the gas phase (Barnes et al. 1994). The method is based on the use of a microcantilever, which adsorbs molecules from the medium under study (Figure 1.26). An IR beam from a tunable laser or IR source (Kim et al. 2012) is absorbed and causes a change in the cantilever bending, which can be measured with an optical system.

Recently, a very interesting schematic has been proposed, *total internal reflection photothermal deflection spectroscopy* (Pleitez et al. 2015). It implements an IR pump/Vis-probe photothermal deflection spectrometry in a prism transparent to IR radiation, in which the optical probe

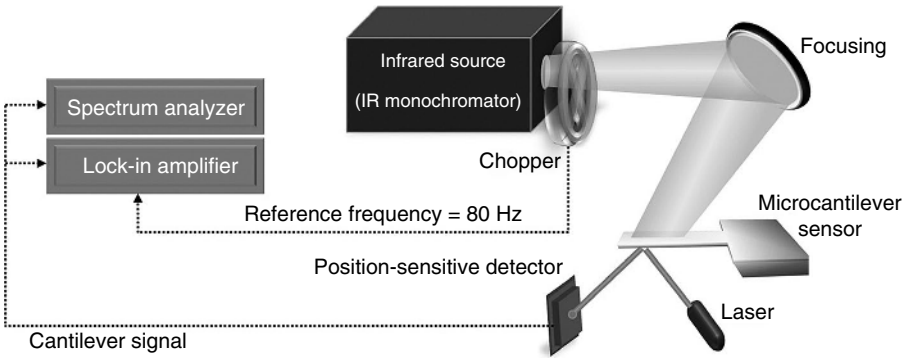

Figure 1.26 Schematic illustration of the setup used for photothermal cantilever deflection spectroscopy experiments. IR light from monochromator is chopped at 80 Hz and focused on the bi-material cantilever by aspherical mirror. The photothermal cantilever deflection signal is measured by optical beam deflection method. Source: Adapted from Kim et al. (2012). Reproduced with permission of The Electrochemical Society.

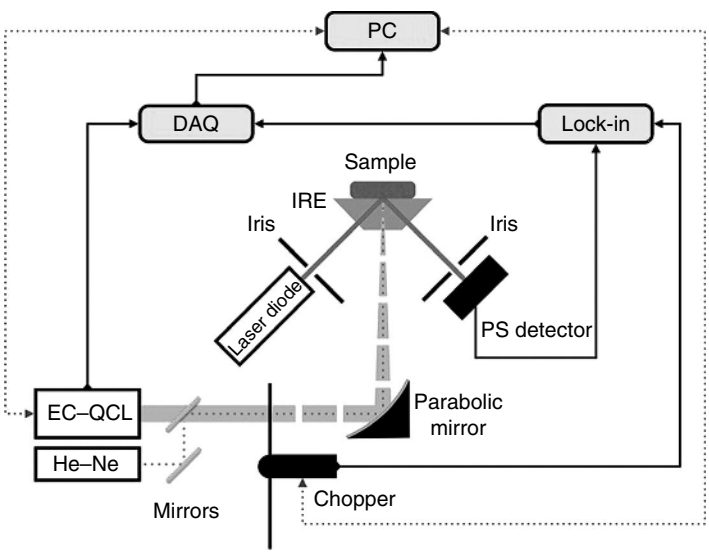

Figure 1.27 TIR-PTDS setup with signal acquisition chain (black arrows) and control/communication structure (grey dotted arrows). The chopper-modulated EC-QCL (Daylight Solutions Uber Tuner 9) acts as a pump laser and is focused to the internal reflection element/sample contact surface to irradiate the sample. The probe beam from a red-emitting diode laser (633 nm, 5 mW, Edmund Optics Model No. 57-108) is guided through the internal reflection element, totally reflected at the interface, and its deflection is measured by the position-sensitive detector (Thorlabs PDQ80A). Iris apertures before and after the internal reflection element help in probe beam collimation. The He–Ne laser is only used for the pump and probe beam alignment. Source: Pleitez et al. (2015). https://pubs.rsc.org/en/content/articlelanding/2015/an/c4an01185f#!divAbstract. Licensed under CC-BY 3.0.

beam experiences total internal reflection (Figure 1.27). The prism is in tight contact with the test material (a liquid or solid film or a tissue), which is heated with a tunable mid-IR quantum cascade laser (QCL). Absorption of excitation radiation results in the formation of the temperature profile in the prism causing the deflection (displacement) of the probe beam, which is measured by a position-sensitive detector.

Hertzberg et al. (2017) showed that this approach outperforms attenuated total reflection (ATR) FTIR spectroscopy for opaque samples providing a higher penetration depth. This method allows fingerprinting of IR-active liquids or solids. Pleitez et al. (2015) claim that another important advantage of the presented approach over traditional mid-IR spectroscopy methods is the ability to obtain the IR information by means of optical (visible) detection, which is generally much cheaper and easier to handle than IR detection.

1.5.9 Photothermal Mirror

In addition to the thermally induced refractive index gradients both in the coupling fluid and within the solid material, photothermal deflection can be applied to investigate a heated surface by exploring its time-dependent thermoelastic displacement under pulsed or continuous laser excitations. This method is referred to as photothermal displacement.

Olmstead et al. (1983) presented the method as a sensitive technique for the determination of optical and thermal properties of solids, surfaces, and thin films. Karner, Mandel, and Träger (1985) used pulsed excitation to investigate real-time transient heating phenomena. Kuo and Munidasa (1990) used a single-beam interferometric scheme to detect the surface displacement of solids, and Li (1990) presented the three-dimensional theory of pulsed photothermal deformation for thin films. Bennis et al. (1998) used the method to measure thermal diffusivity of solids. Cheng and Zhang (1991) and Fang and Zhang (1998) used this method to investigate semiconductors by describing how the photo-displacement, the surrounding thermal lens, and the photoreflectance effects affect the displacement signal. Astrath et al. (2007), Malacarne et al. (2008), and Sato et al. (2008) presented the method to investigate thermo-optical and mechanical properties of semitransparent and opaque materials under pulsed and continuous excitation both experimentally and theoretically. Using a slightly different experimental approach, Astrath et al. (2014) employed this method to measure the surface deformation generated by radiation pressure at air–liquid interfaces induced by continuous and pulsed laser excitation.

The effect is introduced when a focused laser beam excites a solid material and the absorbed energy results in local expansion or contraction and then surface displacement of the solid. Several approaches to detect the surface deformation have been reported for the purpose of the characterization of solid materials. Figure 1.28 shows different apparatuses used for detection.

In the beam deflection scheme (Figure 1.28a), a modulated pump beam irradiates the sample, and the effect is probed by a focused laser beam with a spot size smaller than the heated area. The modulated excitation generates an oscillatory surface displacement that deflects the reflected probe beam at different angles. The signal depends on the deflection of the probe beam that is detected by a position sensor. The deflection signal at the sensor depends on the slope of the displacement, $\partial u_z(r_0)/\partial r$, at the point where the probe beam is reflected (r_0) as

$$S = \gamma \left[2d \frac{\partial u_z(r_0)}{\partial r} + 2u_z(r_0)\sin\theta + O^2 \right] \tag{1.25}$$

where d is the distance from the sample to the sensor, u_z is the surface displacement, θ is the angle of incidence of the probe beam, and γ is the sensor sensitivity. O^2 terms account for the small contributions for the probe beam deflection by the vertical surface displacement.

The interferometric scheme of detection (Figure 1.28b) uses one arm of a conventional Michelson interferometer to detect surface displacement. The signal is stabilized using a piezoelectric (pzt) transducer mounted on other mirror. The intensity of the pump beam incident on

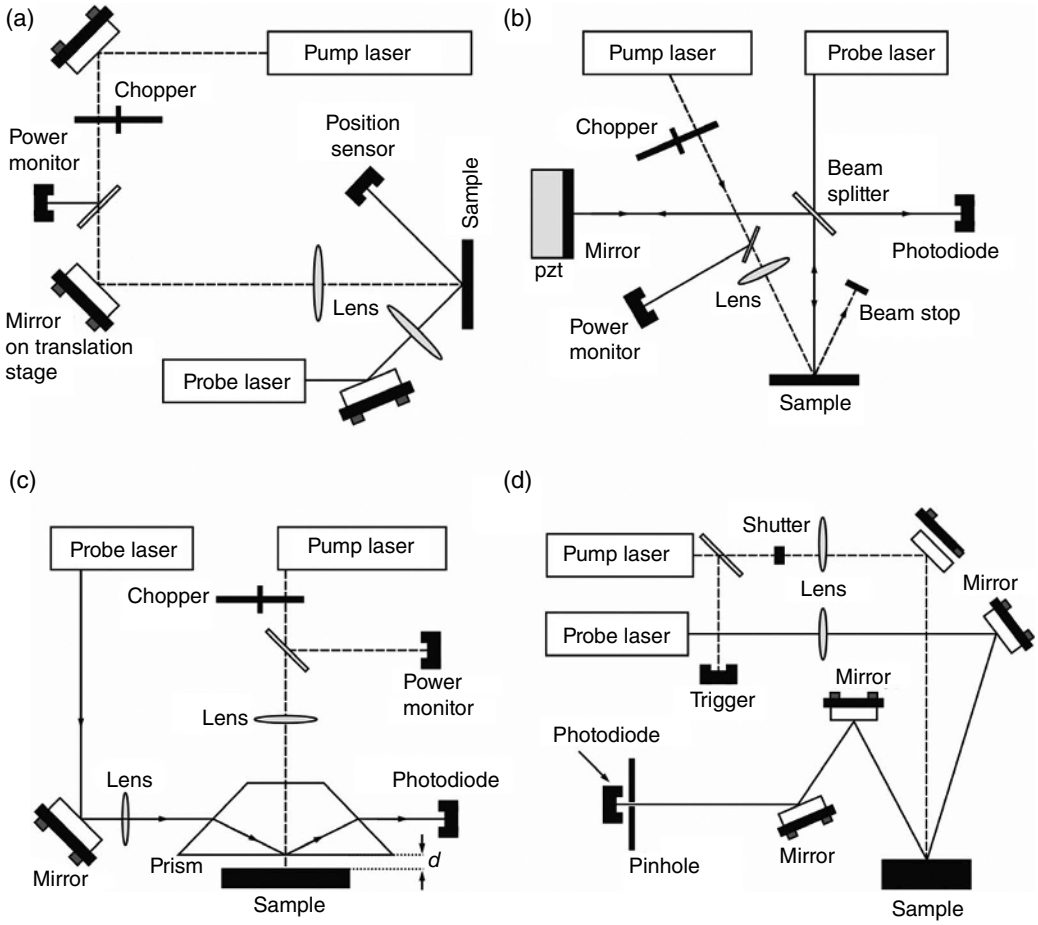

Figure 1.28 Experimental configuration for (a) beam deflection, (b) interferometric, (c) attenuated total reflection detection, and (d) thermal mirror schemes.

the sample is again modulated, causing the surface displacement to rise and fall with an (angular) frequency ω_1, and a small oscillation is applied to the mirror through the pzt at a given frequency. The signal at the photodiode is modulated and depends on the thermoelastic-induced displacement on the sample surface as

$$S(\omega_1) = S_0 \frac{2\pi\delta_1}{\lambda} \sin\left(\frac{4\pi\delta_0}{\lambda}\right) \tag{1.26}$$

The dc path difference, δ_0, is kept near $n\lambda/2$ via a servo loop, λ is the probe beam wavelength, and δ_1 is the amplitude of photothermally induced displacement on the sample. S_0 is the dc signal. Active stabilization of the interferometer is essential to eliminate signal drifts resulting from thermal fluctuations and acoustic disturbances in the interferometer elements.

In the ATR scheme (Figure 1.28c), the photothermal displacement is measured in an ATR geometry, where a transparent prism is placed in close proximity to the sample surface. The width of the gap between the sample and prism varies with the modulated photoinduced

displacement. A probe beam of light internally reflected by the prism will couple some of its energy into the sample via the evanescent field that exists in the gap. Since the evanescent field decays exponentially in the gap as $e^{-2k_\theta d}$, where d is the gap width and $k_\theta = 2\pi/\lambda(n^2\sin^2\theta - 1)^{1/2}$, small changes in the gap width produce large changes in the amount of the probe beam that is coupled into the sample and therefore a change in the intensity of the reflected probe beam. The sensitivity of this method is given by the derivative of the transmission with respect to the gap distance. The ATR method requires careful spacing between the prism and the sample, making implementation difficult in ultrahigh vacuum. It has lower sensitivity than the beam deflection and interferometric methods and thus is not generally as useful as the other two methods in surface experiments. It may, however, be suitable for other applications.

Alternatively, mechanical displacement can be detected by analyzing the focusing or defocusing of the probe beam reflected from the sample surface in the far-field region, as showed in Figure 1.28d. This method has been recently referred to as *PTM spectrometry* and has been introduced under pulsed and continuous wave Gaussian and top-hat laser excitations for the measurement of thermal diffusivity and thermo-optical properties of semitransparent and opaque solids (Astrath et al. 2007).

PTM effect is associated with optical absorption, local heat generation, and thermoelastic expansion. The model takes into account the temperature rise after the absorption of step optical excitation and the thermoelastic effect in the sample by calculating the resulting probe beam optical diffraction, aiming to obtain a simple analytical expression to evaluate the time-resolved behavior of the probe beam intensity at a detector.

A typical two-beam PTM apparatus is described in Figure 1.28d. A continuous or pulsed laser beam excites a solid material, causing a local perturbation to its surface. A second and weak TEM_{00} Gaussian beam, collinearly arranged with the excitation beam, impinges the excited area, probing this deformed area. The detector's plane is in the far field and a pinhole is placed in front of the sensor to detect only the center of the probe beam intensity. In this configuration, several assumptions can be made to simplify the theoretical calculations: (i) the sample dimensions are large compared with the excitation beam radius to avoid edge effects; (ii) the surface displacement along the z direction (normal to the surface) is small compared with the sample thickness (radially semi-infinity sample); and (iii) the absorbed power by the sample is low so that it can be assumed to be uniform along the z-axis.

The temperature change distribution within the solid is given by the solution of the cylindrical symmetric heat conduction differential equation

$$\frac{\partial}{\partial t}\delta T(r,z,t) - D_T\nabla^2\delta T(r,z,t) = \frac{H(r)}{\rho C_P}e^{-\alpha z}f(t) \tag{1.27}$$

where $H(r)$ is the integrated irradiance of the excitation laser beam. The heat conduction equation can be solved using different methods under different boundary and initial conditions. For instance, the temporal distribution of the excitation source may be pulsed, $f(t) = \delta(t)$, or continuous, $f(t) = 1$. The attenuation of light throughout the sample thickness follows the Beer–Lambert law as $e^{-\alpha z}$ and could be simplified in limits of extremely low absorbing materials, $e^{-\alpha z} \to 1$, and opaque samples, $e^{-\alpha z} \to \delta(z)$.

The temperature change in the sample deforms its surface. The theory of thermoelasticity can be used to predict the surface displacement caused by a laser-induced nonuniform temperature distribution. In the quasi-static approximation, the displacement vector, $\mathbf{u} \equiv u(r, z, t)$, is given by the solution of the thermoelastic equation

$$(1-2\nu)\nabla^2\mathbf{u} + \nabla(\nabla.\mathbf{u}) = 2(1+\nu)\beta\nabla\delta T(r,z,t) \tag{1.28}$$

The boundary conditions at the free surface of the sample are over the normal stress components $\sigma_{rz} = 0$ and $\sigma_{zz} = 0$. The solution of Eq. (1.27) can be expressed in cylindrical coordinates, due to the usual geometry of the Gaussian or top-hat pump lasers, by separating the differential equation in a homogeneous (biharmonic) and a nonhomogeneous (Poisson) equation. The Poisson and the biharmonic equations can be solved using the given temperature distribution and the boundary condition over the stress. The normal displacement vector at the sample surface, $u_z(r, z = 0, t)$, contributes to the wavefront distortion caused by the probe beam reflected off the surface. The surface displacement acts as an optical element, causing a phase shift $\Phi(r, t)$ to the reflected probe beam as

$$\Phi(r,t) = \frac{2\pi}{\lambda} 2\, u_z(r,0,t) \tag{1.29}$$

The complex amplitude of an electric field of a TEM_{00} Gaussian probe beam reflected from the perturbed surface and propagating to the detector plane is treated using Fresnel diffraction theory. The relative time-dependent signal of the probe beam at the detector in the far field is

$$S(t) = \left| \int_0^\infty \frac{2r}{w_p^2} \exp\left[-(1 + iz_1/z_c)\frac{r^2}{w_p^2} - i\Phi(r,t) \right] dr \right|^2 \tag{1.30}$$

where w_p is the probe beam radius at the sample surface, z_c is the confocal distance of the probe beam, and z_1 is the distance from the probe beam waist to the sample. Very recently, Photothermal Spectroscopy Corp. (United States) has announced the mIRage IR microscope® claiming to fill the niche of photothermal IR microspectroscopy. The working principle of the instrument is very close to photothermal deflection and PTM measurements and implements their microscale variant. A mid-IR tunable laser beam is mildly focused and hits the test surface. The constituents of the sample in the heated zone absorb the IR radiation, which results in the formation of a photothermal element. This optical element is probed by a more tightly focused visible laser beam collinear with the excitation beam. The tunability of the excitation source provides the selectivity of photothermal measurements and the possibility of spectrum recording. In the case of a nonuniform distribution of IR absorbers, this method provides the imaging of surfaces with a resolution that depends on both the microstructure of the sample and the size of the probe beam. The manufacturer claims the method to have a submicrometer spatial resolution.

Also, one of the latest publications deals with chemical imaging with submicron spatial resolution on the basis of a serial inverted microscope (Li et al. 2017). The authors called the method *epi-detected mid-IR photothermal microscopy*. It is a very interesting implementation of multispectral thermal mirror microspectroscopy. Its capabilities for micro-imaging of complex organic materials (drug tablets) and imaging in live cells (Zhang et al. 2016) are demonstrated.

1.5.10 Photothermal IR Microspectroscopy

Photothermal IR microspectroscopy (or *photothermal-induced resonance spectroscopy*) is somewhat related to photothermal deflection and thermal mirror techniques. However, it has evolved from photothermal effects in atomic force microscopy (AFM) and from the very beginning was oriented toward solving the problems of IR spectroscopy (Hammiche et al. 1996a). In photothermal IR microspectroscopy, the probes similar to those used in various scanning probe microscopic techniques (AFM; scanning thermal microscopy [SThM]; or scanning near-field optical microscopy [SNOM]) are used instead of a standard detector of FTIR spectrometers (Hammiche et al. 1996b,c, 2004b; Pollock, Hammiche, and Song 1996; Price et al. 1999; Reading

et al. 2001). Photothermal IR microspectroscopy is based on the detection by such a probe of the transient and local dilatation of a sample upon resonance heating by a tunable IR laser. The photothermal signal increases when the excitation radiation is absorbed by an absorption line of a sample constituent (Dazzi 2009; Dazzi, Glotin, and Carminati 2010).

Such probes make it possible to obtain spectra with a resolution of down to 20–30 nm, which is much higher than traditional IR spectroscopy, and the resolution does not depend on the wavelength of the IR radiation emitted by the source, but only on the dimensions of the microthermal probe and the thermal properties of the sample. Also, the resolution affects the thermal conductivity of the microthermal probe, the final contact area of the probe and the sample, a complex inhomogeneous temperature distribution in the system, and a change of the absorbed heat flux versus time and wavelength.

The first studies of the possibilities of the method, which is a combination of FTIR spectroscopy and thermal microscopy, refer to 1996 (Hammiche et al. 1996b,c; Pollock, Hammiche, and Song 1996). The probe consisted of a Wollaston filament with a diameter of 75 μm, closed in a loop, with a sharp bend, which plays the role of a temperature sensor. The source of IR radiation was a globar. The sample and the probe were placed in a chamber of a serially produced FTIR spectrometer in the focus of the beam; the schematic of the instrument is shown in Figure 1.29.

In this case, the probe operates in a passive mode, i.e. it records changes in the surface temperature of the sample. As with a probe of any alternative temperature measuring device, e.g. a thermocouple, since the probe is in the focus of the beam, it is inevitable that it is heated not only by the contact with the sample surface, but also directly by the excitation beam, which

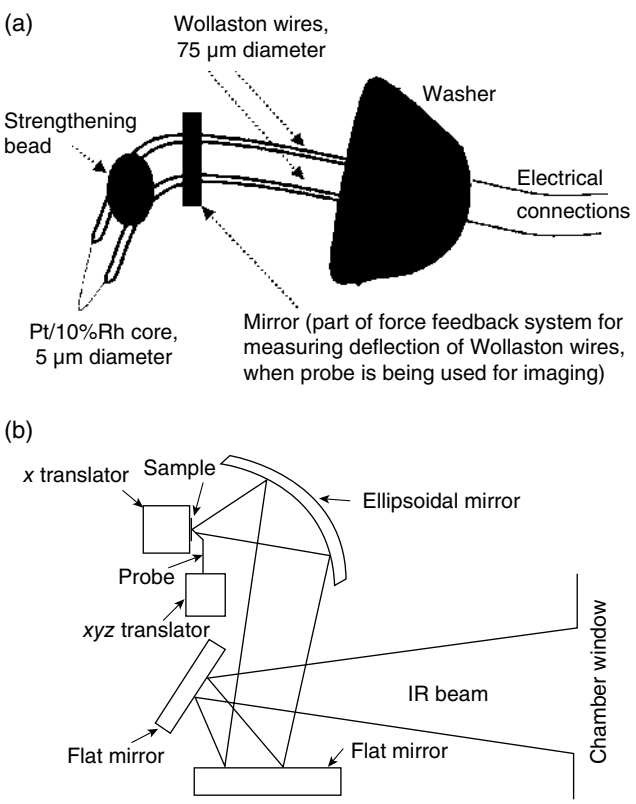

Figure 1.29 The scheme of the probe used in scanning thermal microscopy (a) and the optical scheme of the FTIR spectrometer modified for photothermal FTIR spectroscopy (b). Source: Hammiche et al. (1999). Reproduced with permission of SAGE.

leads to undesirably high background levels. To eliminate the effect, it is suggested to record a contactless background spectrum (the probe does not touch the surface of the sample) and then subtract it from the original spectrum of the sample.

Photothermal spectra are very similar to the reversed traditional IR spectra (Bozec et al. 2001a,b). Minor differences in the shape of the bands are due to sample preparation, according to Bozec et al. (2001b), who recorded photothermal spectra of powders. Also, the changes may be accounted for by the fact that the formation of photothermal spectra is influenced – apart from optical – by thermal factors such as the formation, propagation, and detection of thermal waves. Photothermal spectra can reflect the photothermal saturation due to violation of the linear dependence between the signal and the absorption coefficient at high values. This effect reveals itself as the peak suppression (Bozec et al. 2001b).

One of the reasons for the low quality of the first photothermal spectra is the insufficient irradiance of the IR radiation. Replacing the globar with a more powerful source can significantly shorten the experimental time. Laser sources, for example, a 25 W CO_2 laser (Hammiche et al. 1999) or, more recently a QCL, serve as alternatives. Pollock and Hammiche (2001) introduced a pulsed laser as a tunable source of IR radiation in this technique. Synchrotron IR radiation significantly improves the quality of the spectra (Bozec et al. 2002; Reading et al. 2002).

Hammiche et al. (1999) reported on the use of SThM probes in photothermal IR spectroscopy. Such spectra are distinguished by a high level of noise, but the main characteristic bands, for example, the bands corresponding to the valence C–H vibrations, are clearly visible. The undoubted advantage of this version of the method is the ease of cleaning the probe by transferring the sample material to the solution. A higher resolution than for SThM is provided by a probe whose role is played by a tiny truncated pyramid, on the flat top of which is a 150 × 50 nm palladium sensing element (Bozec et al. 2002). The disadvantages of using a probe of this type include a low signal irradiance compared with an SThM probe.

Further publications (Hammiche et al. 2004a,b, 2005) reported on a method that combines the capabilities of FTIR spectroscopy and atomic force microscope, *photothermal FTIR microspectroscopy* (Figures 1.30 and 1.31). In this case, the SThM probe is located not on a conventional mobile stand but as a part of an AFM microscope. The authors have developed a special design for an embedded AFM device, which can be placed directly in the chamber of most FTIR spectrometers (Hammiche et al. 2004a). The sensitivity of the method, estimated by determining

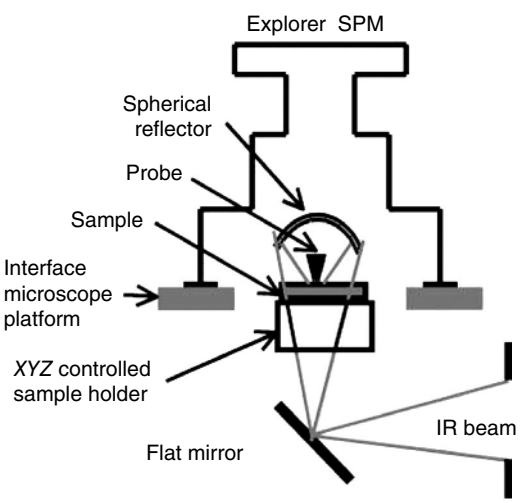

Figure 1.30 The scheme of the experimental setup in the photothermal FTIR microspectroscopy method. Source: Hammiche et al. (2004b). Reproduced with permission of Wiley.

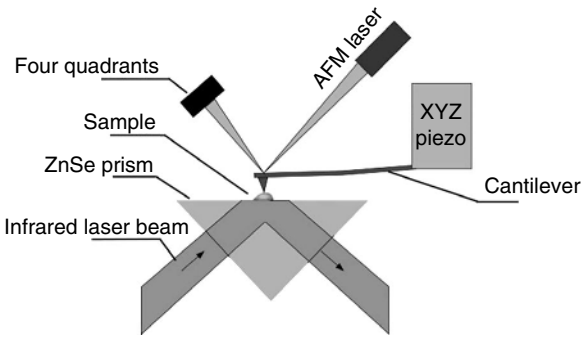

Figure 1.31 Schematics of photothermal FTIR microspectroscopy implemented in tabletop instruments. Source: Dazzi, Glotin, and Carminati (2010). Reproduced with permission of American Institute of Physics.

small amounts of polystyrene microspheres with a diameter of 5 μm on the surface of a salt plate, was found to be higher than the photothermomechanical method using conventional AFM probes as temperature sensors (Hammiche et al. 2004b).

Important features of photothermal FTIR microspectroscopy are common to most state-of-the-art IR techniques: sample preparation is minor or absent, and the technique is nondestructive and capable of testing a variety of objects including heterogeneous samples. As a microspectroscopic technique, it produces images of test materials. At the same time, the method's resolution is higher than for conventional techniques of FTIR spectroscopy (although not for all the samples and a further increase in spatial resolution is awaited). Photothermal IR microspectroscopy is able to handle inhomogeneous samples with simultaneous IR mapping of both inorganic and organic solid-state samples of a submicrometer heterogeneity scale, with a spatial resolution around tens of nanometers (Gasser 2014). It also inherits the sensitivity of photothermal spectroscopy, i.e. the possibility of determining small amounts of components.

The advantages of photothermal FTIR microspectroscopy resulted in the implementation of this and many related techniques in commercially available tabletop instruments produced by Anasys Instruments (recently, Bruker NANO Group), which are used in many applied studies (Chae et al. 2015; Ghosh et al. 2015). Morsch, Bastidas, and Rowland (2017) published a focused overview of the use of photothermal FTIR microspectroscopy in interface and materials science.

1.5.11 Photothermal Radiometry

Another widespread photothermal method is PTR. It was introduced into the practice of photothermal measurements by Tam and Sullivan (1983) and Imhof et al. (1984). In PTR, the sample is excited with an optical source and the IR emission is monitored. The IR emission is related to the sample temperature by the black-body radiation law (Ingle and Crouch 1988):

$$B(\lambda, T) = \varepsilon(\lambda) \frac{2hc^2}{\lambda^5} \frac{1}{e^{hc/\lambda k_B T} - 1} \tag{1.31}$$

where $B(\lambda,T)$ (W sr^{-1} m^{-2}) is the radiant emissivity, h (J s) is Planck's constant, k_B (J K^{-1}) is Boltzmann's constant, and $\varepsilon(\lambda)$ is the sample emissivity. For samples at thermal equilibrium, $\alpha(\lambda) = \varepsilon(\lambda)$. The relative change in spectral radiance with respect to temperature is

$$\frac{\delta B(\lambda, T)}{B(\lambda, T)} = \frac{hc}{\lambda k_B T^2} \frac{\alpha(\lambda)}{1 - e^{-ch/\lambda k_B T}} \delta T \tag{1.32}$$

In the mid-IR region, $hc/\lambda kT < 1$, and for pulsed laser excitation

$$\frac{\delta B(\lambda_{em}, T)}{B(\lambda_{em}, T)} \approx \frac{hc\alpha(\lambda_{em})}{\lambda_{em} k_B T^2} \frac{2\alpha(\lambda_{ex})Q}{\pi w^2 \rho C_P} \tag{1.33}$$

where λ_{em} is the emission wavelength and λ_{ex} is the excitation wavelength. The important features of this equation are that (i) the relative radiance increases with excitation laser energy and absorption coefficient, (ii) decreases with equilibrium temperature, and (iii) decreases with increasing wavelength and that (iv) since $\alpha(\lambda_{em})$ and $\alpha(\lambda_{ex})$ are both proportional to number density or concentration, the relative emission signal decreases as the square of the number density. The latter suggests that this method will not be as sensitive as other photothermal techniques since the sensitivity decreases with decreasing α.

This method of analysis has a long and somewhat obscured history. The advent of lasers and cryogenic IR detectors resulted in several studies of IR emission from excited gas samples. The method used to study gas samples is called laser-induced fluorescence (Hocker et al. 1966; Yardley and Moore 1966; Stephenson, Wood, and Moore 1968, to name a few). These pioneering studies used pulsed IR lasers to excite specific vibrational modes while monitoring IR fluorescence at wavelengths different from that used for excitation. Time-resolved fluorescence emission studies were performed to reveal the excited state vibrational lifetimes of low pressure gas species. These lifetimes are a direct measure of the thermalization time of sample. With the notable exception of the work by Belz et al. (1987), IR emission methods have been neglected for gas analysis although their utility is apparent.

PTR has been recognized as an important tool for surface studies and materials analysis (Nordal and Kanstad 1979). The solid being analyzed is treated as a black-body emitter. The total surface emission will follow the Stefan–Boltzmann law. The relative temperature-dependent change in surface emittance, e.g. integrating over wavelength, is simply

$$\frac{\delta M(T)}{M(T)} = 4\frac{\delta T}{T} \tag{1.34}$$

where $M(T)$ (W m^{-2}) is the temperature-dependent emittance of the surface and ΔT is induced by the photothermal effect. The temperature change can be produced by either pulsed or chopped excitation sources. This method is not very sensitive and rather large temperature changes have to be induced in the samples to obtain good thermal images. The thermal images are not a function of surface topography (unless three-dimensional imaging optics is used). The images will only depend on the optical absorption coefficient and the heat capacity of the sample. Time- or phase-dependent analysis of the emittance yields information regarding thermal conductivity. If the integrated emission data is not processed as indicated in the above equation, the thermal image will also be a function of the topographical emissivity of the material. Tam (1985) has examined the use of PTR for solid sample analysis and has reviewed the literature regarding applications of the method (Tam 1983, 1986, 1989). Busse (1989) has covered this in reviews of nondestructive materials evaluation using photothermal methods.

The detection of radiation using a standard mercury cadmium telluride (MCT) detector for IR spectroscopy is the basis of several advanced PTR techniques (Jeon, Mandelis, and Abrams 2003; Liu, Baddour, and Mandelis 2003; Li, Mandelis, and Kish 2004). In combination with a spatial scanning unit, the method renders photothermal images of the sample. A very interesting version of PTR developed specifically for the study of semiconductor materials is *IR photocarrier radiometry*. It also records IR radiation emitted by the sample, but unlike PTR, it is not of thermal origin but is caused by the laser excitation of the additional charge carriers (Batista, Mandelis, and Shaughnessy 2003, 2005; Mandelis, Batista, and Shaughnessy 2003; Batista

et al. 2004, 2005; Li et al. 2004a,b; Li, Shaughnessy, and Mandelis 2005a,b; Mandelis 2005; Mandelis et al. 2005a,b,c; Shaughnessy et al. 2005, 2006; Shaughnessy, Mandelis, and Batista 2005; Shaughnessy and Mandelis 2006; Mandelis and Tolev 2008; Mandelis and Xia 2008).

The concept of the method consists in irradiating the sample with pulses whose energy exceeds the width of the bandgap of the semiconductor (Chen et al. 1993). As a result, additional charge carriers (electron–hole pairs) appear at the sample surface, whose lifetime is further determined from the PTR signal behavior. The resolution is determined by the dynamic range of the data processing system only. IR photocarrier radiometry makes it possible to determine carrier mobility, lifetime, diffusion coefficients, and surface recombination rates (Batista, Mandelis, and Shaughnessy 2003; Mandelis, Batista, and Shaughnessy 2003).

The experimental design of the IR photocarrier radiometry measurements is similar to that of PTR with semiconductors. The feature of the method is in the signal detection system (Batista, Mandelis, and Shaughnessy 2003; Mandelis, Batista, and Shaughnessy 2003). Instead of an MCT detector with a spectral window of 2–12 μm, an InGaAs detector is used, whose transmission bandwidth is 0.8–1.8 μm. Under these conditions, the signal component caused by thermal waves is completely suppressed. In addition, an InGaAs detector, in contrast to an MCT detector cooled with liquid nitrogen, allows measurements at room temperature. Mandelis, Batista, and Shaughnessy (2003) showed that the amplitude and phase of the IR photocarrier radiometry signal, in contrast to PTR, are practically independent from the modulation frequency of the laser pulse in the 10 Hz–100 kHz range and are characterized by the best signal-to-noise ratio.

Imhof, McKendrick, and Xiao (1995) introduced a PTR technique called *opto-thermal transient emission radiometry* (OTTER) (Figure 1.32). OTTER provides noninvasive and noncontact

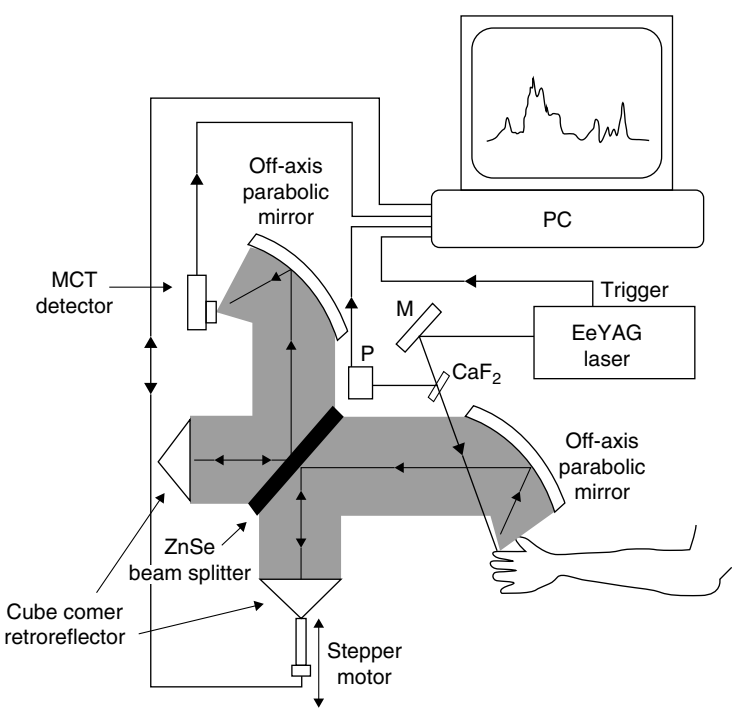

Figure 1.32 Schematics of the experimental setup in the method of thermal emission decay FTIR spectroscopy (Imhof, McKendrick, and Xiao 1995; Notingher et al. 2001, 2003; Notingher and Imhof 2004). M is a mirror; P is a piezoelectric sensor. Source: Reproduced with permission from Wiley.

recording of absorption spectra of any surface. It is based on pulsed optical heating of the region near the sample surface and produces transient thermal emission spectra. OTTER works in IR (a 2.94 μm Er:YAG laser or a QCL laser) or UV/Vis (Nd:YAG or OPO [optical parametric oscillator] lasers) ranges. As in other PTR methods, only the absorbed light produces signal in OTTER, due to the use of an MCT detector, while remitted (reflected and backscattered) and scattered radiation make negligible contributions to the signal. The method makes it possible to obtain two types of spectra – transient (averaged signal over a certain time produced at a certain rate after irradiation with a laser pulse) and attenuation spectra – which are independent of the absorbed energy (Xiao 2016). Transient spectra contain information on spectral changes that depend on the depth below the surface of the sample. Instrumental design of the method includes a radiation source (OPO laser), a spectrum analyzer (usually an interferometer), and an MCT detector.

On the basis of OTTER, the method of *thermal emission decay FTIR spectroscopy* was introduced (Imhof, McKendrick, and Xiao 1995; Notingher et al. 2001, 2003; Notingher and Imhof 2004). It is based on the ratio of absorption and emission in the theory of thermal radiation and was developed for studying rough surfaces of complex and layered materials without sample preparation, especially human skin and nails. The principle of the method consists in irradiating the sample surface with laser pulses, after which, as a result of excitation and relaxation processes, the sample emits thermal radiation, which serves as a signal.

In OTTER and thermal emission decay FTIR spectroscopy, the signal is a decay signal, and it depends on the detection wavelength and the constituents of the material. Most common measured components are water concentration and its distribution in skin or solvent/medicine concentration information within skin (9.5 μm). Various mathematical models (Xiao, Cowen, and Imhof 2001, 2003; Cui, Xiao, and Imhof 2005) have been developed to render the reliable distribution of water in the stratum corneum or solvent (such as ethylene glycol) depth profiles in the stratum corneum (Xiao 2016).

OTTER and thermal emission decay FTIR spectroscopy satisfy the basic conditions necessary for performing *in vivo* experiments: rapidity (registration of the spectrum takes about 15 min), nondestructibility (the sample not only does not break down, but does not undergo any changes, as the temperature rise of the investigated skin area is less than 1 °C), noncontact character, and insensitivity to displacements and irregularities of the sample.

1.5.12 Historic Summary

The important discoveries in the history of photothermal spectroscopy are given in Table 1.3. Many of these discoveries were made possible by using lasers. Although lasers do not have to be used to excite samples, the signals thereby obtained are much greater than those obtained using incoherent light sources. Historically, the birth of high sensitivity photoacoustic and photothermal spectroscopies can be traced back to the laser. The first application of the photoacoustic effect was that of A. G. Bell (1880), while chemical analysis applications of photoacoustic spectroscopy can be traced back to Viengerov (1938). The first photothermal method was discovered by Leite, Moore, and Whinnery (1964) when they found an intracavity sample laser-based apparatus gave rise to photothermal blooming, the photothermal lens. Some time later Kreuzer (1971) showed that photoacoustic spectroscopy could be used for sensitive analysis when laser light sources were utilized.

The reasons why lasers have made such an impact on high sensitivity spectroscopy are because they possess a high spectral brightness and they have outputs that are coherent. The high spectral brightness allows high powers or energies to be imparted to the sample. The coherence, in particular the spatial coherence, allows this power or energy to be delivered to small volumes.

Table 1.3 Major developments in the history of photothermal spectroscopy.

1880	Photoacoustic effect used for photophone by Bell
1938	Viengerov uses photoacoustic effect for gas-phase chemical analysis
1964	Photothermal lens is used to measure optical absorptions by Leite et al.
1968	McLean et al. use interferometry to monitor photothermal effect
1969	Longaker and Litvak find thermal and acoustic components in photothermal effect. Use of a pulsed excitation laser
1971	Kreuzer demonstrates sensitive gas-phase detection with photoacoustic spectroscopy
1972	Grabiner et al. use two-laser pulsed excitation photothermal lens method for excited state relaxation kinetic measurements
1973	Hu and Whinnery develop extracavity single-laser photothermal lens spectroscopy
1976	Long et al. measure excitation spectra with two-laser photothermal lens spectroscopy
1977	Twarowski and Kliger develop the theory for pulsed laser photothermal lens and measure two-photon absorption spectra of benzene; Patel et al. report 10^{-10} cm^{-1} detection limits for gas-phase photoacoustic measurements
1979	Dovichi and Harris use the single-laser photothermal lens technique for chemical analysis and introduce the enhancement factor; Boccara et al. report photothermal deflection
1981	Murphy and Aamodt report thermal images using photothermal deflection; Davis and Petuchowski report 10^{-10} cm^{-1} detection limits for gas-phase photothermal interferometry measurements; Dovichi and Harris report 10^{-7} cm^{-1} detection limits with single-laser solution-phase photothermal lens
2001	Tokeshi et al. report sub-yoctomole ($<10^{-24}$ mol) detection limits, or 0.4–3.4 molecules in the excitation beam, using thermal lens microscopy but did not show single-molecule detection (Tokeshi et al. 2001)
2010	Gaiduk et al. achieve single-molecule detection using photothermal microspectroscopy by observing optical bleaching. There have been several similar reports since this time (Gaiduk et al. 2010a,b)

The signals in both photoacoustic and photothermal spectroscopies are enhanced with smaller excitation volumes.

1.6 Some Important Features of Photothermal Spectroscopy

We have now come to regard photothermal spectroscopy as a group of high sensitivity techniques that can be used for chemical and materials analysis. Photothermal signals arise from optical absorption in a sample. However, photothermal spectroscopy techniques have sensitivities far exceeding those of conventional absorption spectrophotometry. The reason for the high sensitivity of photothermal spectroscopy is that it is an indirect technique for measuring optic absorption. For an analyte with less than unit fluorescence quantum yield, electromagnetic energy absorbed and not lost by subsequent emission results in an increase in the energy of the sample. Energy absorbed and not subsequently lost by emission is usually randomized, resulting in sample heating. The photothermal spectroscopy signal is derived from this heating.

A variety of methods are used to monitor sample heating. Calorimetric or thermometric methods use temperature transducers to measure sample temperature. The method of photoacoustic spectroscopy uses a pressure transducer to monitor the pressure wave associated with rapid sample heating. Photothermal emission radiometry uses photometric transducers to monitor changes in the sample IR emission associated with heating. Photothermal interferometry, photothermal deflection, photothermal lensing, and photothermal diffraction spectrometry

are all photothermal techniques that are based on monitoring refractive index changes associated with sample heating.

The distinctions between all but the calorimetric and PTR techniques are lessening. The connection between photothermal and photoacoustic spectroscopies is apparent. Signals attributable to the photoacoustic effect are seen in photothermal spectroscopy experiments though the converse is not true. A pressure transducer placed far from the excitation source will not respond to the thermal perturbation. Photoacoustic spectroscopy apparatuses may use probe lasers to detect the acoustic wave. This eliminates the use of pressure transducers that may have low response times. However, photoacoustic deflection spectroscopy is orders of magnitude less sensitive than photothermal lensing or deflection.

Accurate theories for describing photothermal spectroscopy signals have been developed. In most cases, these theories take into account the thermodynamics, hydrodynamics, and optics of the experimental apparatuses. In some cases, for example, in the single-laser photothermal lens apparatus, the absorption coefficient may be obtained directly from the signal if the thermodynamic and optical parameters are known well enough. In most other cases the signal magnitude has an instrumental factor that must be determined using samples of known absorbance in sample matrices that are identical to those of the unknown sample.

A summary of the best absorption coefficient detection limits for photothermal and photoacoustic methods is given in Table 1.4. The detection limits are given in inverse energy or power units since all photothermal methods scale proportional to the excitation. For continuous excitation, lock-in amplifier signal processing is generally used to recover the oscillatory signal. The noise power is proportional to the bandwidth of the measurement; these detection limits are inversely proportional to the square root of the measurement bandwidth. The theoretical detection limits are based on thermodynamic fluctuations in sample pressure (Slatkine 1981). The noise equivalent power, NEP (W $Hz^{-1/2}$), is

$$\mathrm{NEP} \approx \left(4k_B T^2 \delta f \frac{2\pi r l \kappa}{\sqrt{4D_T/f}} \right)^{1/2} \tag{1.35}$$

where k_B is Boltzmann's constant, f is the frequency, δf is the measurement bandwidth, r and l are the radius and length of the sample cell, κ is thermal conductivity, and D_T is the thermal diffusivity.

Table 1.4 Absorption coefficient detection limits using photothermal and photoacoustic methods for pulsed α (J^{-1} cm^{-1}) and chopped α (W^{-1} cm^{-1} $Hz^{-1/2}$) sources.

	Photothermal spectroscopy[a]		Photoacoustic spectroscopy[b]		Theoretical photoacoustic[c]		
	Pulsed	CW	Pulsed	CW	Pulsed	CW	Typical background[d]
Gas	10^{-12}	10^{-10}	10^{-10}	10^{-10}	10^{-12}	10^{-11}	10^{-5} (IR)
Liquid	10^{-10}	10^{-8}	10^{-9}	10^{-6}	10^{-10}	10^{-9}	10^{-6} (Vis)
Solid	—	—	10^{-7}	10^{-5}	—	10^{-6}	10^{-5} (Vis)

[a] Section 1.5 of this book and Dovichi (1987); α detection limits scaled to W^{-1} or J^{-1}.
[b] Tam (1983) and Zharov and Letokhov (1986).
[c] Theoretical absorption detections limits summarized by Zharov and Letokhov (1986).
[d] Background absorptions typical of water vapor at 10 μm, solvent overtones in liquids, and impurities in fused silica in the visible.

The fluctuations that ultimately limit photoacoustic spectroscopy should also place a lower bound on photothermal spectroscopy since pressure and density are related:

$$\delta\rho = \left(\frac{\partial\rho}{\partial P}\right)_T \delta P = \rho_0 K_T \delta T \tag{1.36}$$

where K_T (Pa^{-1}) is the isothermal compressibility.

For gas- and solution-phase analysis, photothermal and photoacoustic spectroscopy apparatuses have been developed, which yield signals that are close (one to two orders of magnitude) to the theoretical limits of absorbance detection. Quantitative work in solid analysis is nearly impossible because of the difficulty in preparing standard samples. These detection limits are lower than the background absorbance of water and other trace gases in the atmosphere and of solvents used to host the analyte. The lower detection limits are obtained for gas samples because of reduced matrix absorptions and favorable thermodynamic parameters. The problem with the sensitive absorbance measurement methods lies not so much in the measurement of low absorption coefficients, but rather in discriminating the low analyte from that of the solvent or other species in the sample.

From these and other examples, it is clear that photothermal spectroscopy is a valuable tool that can be used to solve a variety of chemical and materials analysis problems. Some salient features are as follows:

1) The sensitivity of photothermal spectroscopy is theoretically enhanced over that of conventional absorption spectrophotometry. This theoretical enhancement has been realized, and absorbance detection limits of approximately 10^{-7} in liquids and approximately 10^{-10} absorbance units in gases are possible. High sensitivity has allowed the measurement of weak optical absorbances in pure samples and trace analysis, and in volume-restricted samples.
2) The Photothermal spectroscopy signal contains both magnitude and dynamic (time-dependent) components. The magnitude component is most important for quantitative absorption studies, spectroscopy, trace analysis, chromatography, etc. The dynamic component is important in qualitative analysis, material composition, chemical kinetics, etc.
3) Photothermal signals are inversely proportional to the excitation volume. This arises not only because of the higher temperature changes that can be induced with a given power or energy but also because photothermal signals are usually derived from a spatial gradient in the resulting refractive index change. The small volume character of photothermal spectroscopy has led to its use for microanalysis and effluent detection in chromatography.

References

Alves, S., Bourdon, A., and Neto, A.M.F. (2003). *J. Opt. Soc. Am., B: Opt. Phys.* **20** (4): 713–718.
Alves, S.I., Bourdon, A., and Neto, A.M.F. (2005). *J. Magn. Magn. Mater.* **289**: 285–288.
Andrade, A.A., Catunda, T., Lebullenger, R. et al. (1998). *Electron. Lett.* **34** (1): 117–119.
Andrade, A.A., Tenorio, E., Catunda, T. et al. (1999). *J. Opt. Soc. Am., B: Opt. Phys.* **16** (3): 395–400.
Andrade, A.A., Catunda, T., Lebullenger, R. et al. (2000). *J. Non Cryst. Solids* **273** (1–3): 257–265.
Aota, A. and Kitamori, T. (2010). Microunit operations and continuous flow chemical processing. In: *Micro Systems and Devices for (Bio)Chemical Processes* (ed. J.C. Schouten), 1–36. Oxford: Academic Press.
Astrath, N.G.C., Malacarne, L.C., Pedreira, P.R.B. et al. (2007). *Appl. Phys. Lett.* **91**: 191908.
Astrath, N.G.C., Malacarne, L.C., Baesso, M.L. et al. (2014). *Nat. Commun.* **5** (4363).

Barker, J.R. and Rothem, T. (1982). *Chem. Phys.* **68**: 331.
Barker, J.R. and Toselli, B.M. (1989). *Photothermal Investigations in Solids and Fluids* (ed. J.A. Sell). New York: Academic Press.
Barnes, J.R., Stephenson, R.J., Welland, M.E. et al. (1994). *Nature* **372** (6501): 79–81.
Batista, J., Mandelis, A., and Shaughnessy, D. (2003). *Appl. Phys. Lett.* **82** (23): 4077–4079.
Batista, J., Mandelis, A., Shaughnessy, D., and Li, B.C. (2004). *Appl. Phys. Lett.* **85** (10): 1713–1715.
Batista, J., Mandelis, A., and Shaughnessy, D. (2005). *J. Phys. IV* **125**: 443–445.
Batista, J., Mandelis, A., Shaughnessy, D., and Li, B. (2005). *J. Phys. IV* **125**: 557–559.
Beitz, J.V., Doxtader, M.M., Maroni, V.A. et al. (1990). *Rev. Sci. Instrum.* **61**: 1395.
Bell, A.G. (1880). *Am. J. Sci.* **20**: 305.
Bell, A.G. (1881). *Philos. Mag.* **11**: 510.
Belz, H.H., Gutberlet, H., Schallert, B., and Schrader, B. (1987). *Appl. Spectrosc.* **41**: 1009.
Bennis, G.L., Vyas, R., Gupta, R. et al. (1998). *J. Appl. Phys.* **84**: 3602.
Berciaud, S., Cognet, L., Blab, G.A., and Lounis, B. (2004). *Phys. Rev. Lett.* **93** (25): 257402.
Berciaud, S., Lasne, D., Blab, G.A. et al. (2006). *Phys. Rev. B* **73** (4): 045424.
Berciaud, S., Cognet, L., Poulin, P. et al. (2007). *Nano Lett.* **7** (5): 1203–1207.
Berciaud, S., Cognet, L., and Lounis, B. (2008). *Phys. Rev. Lett.* **101** (7): 077402.
Betteridge, C.M. and Meylor, P.J. (1984). *CRC Crit. Rev. Anal. Chem.* **14**: 267.
Bialkowski, S.E. (1988). *Chem. Phys. Lett.* **151**: 88.
Bialkowski, S.E. (1998). *Trends Analyt. Chem.* **17** (8–9): 520–532.
Bialkowski, S.E. and He, Z.-F. (1988). *Anal. Chem.* **60**: 2674.
Bialkowski, S.E., Gu, X., Poston, P.E., and Powers, L.S. (1992). *Appl. Spectrosc.* **46**: 1335.
Blab, G.A., Cognet, L., Berciaud, S. et al. (2006). *Biophys. J.* **90** (1): L13–L15.
Boccara, A.C., Fournier, D., and Badoz, J. (1979). *Appl. Phys. Lett.* **36**: 130.
Boccara, A.C., Fournier, D., Jackson, W., and Amer, N.M. (1980). *Opt. Lett.* **5**: 377.
Boyer, D., Tamarat, P., Maali, A. et al. (2002). *Science* **297** (5584): 1160–1163.
Bozec, L., Hammiche, A., Pollock, H.M., and Conroy, M. (2001a). *Anal. Sci.* **17**: S494–S496.
Bozec, L., Hammiche, A., Pollock, H.M. et al. (2001b). *J. Appl. Phys.* **90** (10): 5159–5165.
Bozec, L., Hammiche, A., Tobin, M.J. et al. (2002). *Meas. Sci. Technol.* **13** (8): 1217–1222.
Brazhnik, P.K. and Novikov, M.A. (1991a). *Opt. Spektrosk.* **70** (2): 453–458.
Brazhnik, P.K. and Novikov, M.A. (1991b). *Opt. Spektrosk.* **71** (3): 502–506.
Brazhnik, P.K., Novikov, M.A., and Pushkin, A.A. (1990). *Opt. Spektrosk.* **68** (3): 631–635.
Brochard, P., GrolierMazza, V., and Cabanel, R.J. (1997). *Opt. Soc. Am., B: Opt. Phys.* **14** (2): 405–414.
Busse, G. (1989). *Photoacoustic, Photothermal and Photochemical Processes at Surfaces and Thin Films* (ed. P. Hess). New York: Springer-Verlag.
Castillo, M.D.I., Sanchezmondragon, J.J., and Stepanov, S.I. (1995). *Optik* **100** (2): 49–56.
Catunda, T., Baesso, M.L., Messaddeq, Y., and Aegerter, M.A. (1997). *J. Non Cryst. Solids* **213**: 225–230.
Chae, J., Dong, Q., Huang, J., and Centrone, A. (2015). *Nano Lett.* **15** (12): 8114–8121.
Chen, Z.H., Bleiss, R., Mandelis, A. et al. (1993). *J. Appl. Phys.* **73** (10): 5043–5048.
Cheng, J.C. and Zhang, S.Y. (1991). *J. Appl. Phys.* **70**: 7007.
Cognet, L., Tardin, C., Boyer, D. et al. (2003). *Proc. Natl. Acad. Sci. U. S. A.* **100** (20): 11350–11355.
Collier, R.J., Burckhardt, C.B., and Lin, L.H. (1971). *Optical Holography*. New York: Academic Press.
Cui, Y., Xiao, P., and Imhof, R.E. (2005). *Int. J. Thermophys.* **26** (1): 213–220.
Davis, C.C. and Petuchowski, S.J. (1981). *Appl. Optics* **20**: 2539.
Dazzi, A. (2009). Photothermal induced resonance. Application to infrared spectromicroscopy. In: *Thermal Nanosystems and Nanomaterials* (ed. S. Volz), 469–503. Berlin: Springer.
Dazzi, A., Glotin, F., and Carminati, R. (2010). *J. Appl. Phys.* **107** (12): 124519.
Dovichi, N.J. (1987). *CRC Crit. Rev. Anal. Chem.* **17**: 357.

Dovichi, N.J. (1990). *Rev. Sci. Instrum.* **61**: 3653.
Dovichi, N.J. and Harris, J.M. (1979). *Anal. Chem.* **51**: 728.
Dovichi, N.J. and Harris, J.M. (1981). *Anal. Chem.* **53**: 106.
Eichler, H.J., Günter, P., and Pohl, D.W. (1986). *Laser-Induced Dynamic Gratings*. New York: Springer-Verlag.
Falconieri, M.J. (1999). *Opt. A: Pure Appl. Opt.* **1** (6): 662–667.
Falconieri, M., D'Amato, R., Furlani, A., and Russo, M.V. (2001). *Synth. Met.* **124** (1): 217–219.
Fang, H.L. and Swofford, R.L. (1983). *Ultrasensitive Laser Spectroscopy* (ed. D.S. Kliger). New York: Academic Press.
Fang, J.W. and Zhang, S.Y. (1998). *Appl. Phys. B* **67**: 633.
Fotiou, F.K. and Morris, M.D. (1986). *Appl. Spectrosc.* **40**: 704.
Fotiou, F.K. and Morris, M.D. (1987). *Anal. Chem.* **59**: 185.
Fournier, D. and Boccara, A.C. (1988). *Photothermal Investigations in Solids and Fluids* (ed. J.A. Sell). New York: Academic Press.
Fournier, D., Boccara, A.C., Amer, N.M., and Gerlach, R. (1980). *Appl. Phys. Lett.* **37**: 519.
Franko, M. (2008). *Appl. Spectrosc. Rev.* **43** (4): 358–388.
Franko, M. and Tran, C.D. (1996). *Rev. Sci. Instrum.* **67** (1): 1–18.
Franko, M. and Tran, C.D. (2006). *Thermal Lens Spectroscopy, Encyclopedia of Analytical Chemistry*. Chichester: Wiley.
Friedrich, D.M. (1983). *Ultrasensitive Laser Spectroscopy* (ed. D.S. Kliger). New York: Academic Press.
Gaiduk, A., Yorulmaz, M., Ruijgrok, P.V., and Orrit, M. (2010a). *Science* **330**: 353.
Gaiduk, A., Ruijgrok, P.V., Yorulmaz, M., and Orrit, M. (2010b). *Chem. Sci.* **1**: 343.
Galanzha, E.I. and Zharov, V.P. (2012). *Methods* **57** (3): 280–296.
Ganeev, R.A., Ryasnyansky, A.I., Redkorechev, V.I. et al. (2003). *Optics Comm.* **225** (1–3): 131–139.
Gasser, G. (2014). *Inorganic Chemical Biology: Principles, Techniques and Applications*. Chichester: Wiley.
Georges, J. (1999). *Talanta* **48** (3): 501–509.
Ghaleb, K.A. and Georges, J. (2004). *Spectrochim. Acta A* **60** (12): 2793–2801.
Ghosh, S., Kouamé, N.A., Ramos, L. et al. (2015). *Nat. Mater.* **14**: 505.
Gordon, J.P., Leite, R.C.C., Moore, R.S. et al. (1964). *Bull. Am. Phys. Soc.* **9**: 501.
Gordon, J.P., Leite, R.C.C., Moore, R.S. et al. (1965). *J. Appl. Phys.* **36**: 3.
Goswami, D. (2006). *Opt. Commun.* **261** (1): 158–162.
Grabiner, F.R., Siebert, D.R., and Flynn, G.W. (1972). *Chem. Phys. Lett.* **17**: 189.
Gupte, S.S., Marcano, O., Pradhan, R.D. et al. (2001). *J. Appl. Phys.* **89** (9): 4939–4943.
Hammiche, A., Reading, M., Pollock, H.M. et al. (1996a). *J. Rev. Sci. Instrum.* **67** (12): 4268–4274.
Hammiche, A., Song, M., Pollock, H.M., and Hourston, D.J. (1996b). *Abstr. Pap. Am. Chem. Soc.* **212**: 186-PMSE.
Hammiche, A., Song, M., Pollock, H.M. et al. (1996c). *Abstr. Pap. the Am. Chem. Soc.* **212**: 278-POLY.
Hammiche, A., Pollock, H.M., Reading, M. et al. (1999). *Appl. Spectrosc.* **53** (7): 810–815.
Hammiche, A., Bozec, L., German, M.J. et al. (2004a). *Spectroscopy* **19** (2): 20–42.
Hammiche, A., Bozec, L., Pollock, H.M. et al. (2004b). *J. Microsc. (Oxford)* **213**: 129–134.
Hammiche, A., German, M.J., Hewitt, R. et al. (2005). *Biophys. J.* **88** (5): 3699–3706.
Harris, J.M. (1986). *Opt. News* **8** (October).
Hertzberg, O., Bauer, A., Kuderle, A. et al. (2017). *Analyst* **142** (3): 495–502.
Herzfeld, K.F. and Litovitz, T.A. (1959). *Absorption and Dispersion of Ultrasonic Waves*. New York: Academic Press.
Hess, P. (ed.) (1989a). *Photoacoustic, Photothermal and Photochemical Processes in Gases*. New York: Springer-Verlag.

Hess, P. (ed.) (1989b). *Photoacoustic, Photothermal and Photochemical Processes at Surfaces and Thin Films*. New York: Springer-Verlag.
Hibara, A., Sato, K., Hisamoto, H. et al. (2001a). *Prog. Nat. Sci.* **11**: S237–S241.
Hibara, A., Tokeshi, M., Uchiyama, K. et al. (2001b). *Anal. Sci.* **17** (1): 89–93.
Hiki, S., Tokeshi, M., Hibara, A., and Kitamori, T. (2003). *Bunseki Kagaku* **52** (8): 569–574.
Hisamoto, H., Horiuchi, T., Tokeshi, M. et al. (2001). *Anal. Chem.* **73** (6): 1382–1386.
Hocker, L.O., Kovacs, M.A., Rhodes, C.K. et al. (1966). *Phys. Rev. Lett.* **17**: 233.
Hu, C. and Whinnery, J.R. (1973). *Appl. Opt.* **12**: 72.
Hutchins, D.A. and Tam, A.C. (1986). *IEEE Trans. Ultrason. Ferroelectr. Freq. Control* **UFFC-33**: 429.
Imangholi, B., Hasselbeck, M.P., and Sheik-Bahae, M. (2003). *Opt. Comm.* **227** (4–6): 337–341.
Imhof, R.E., Birch, D.J.S., Thornley, F.R. et al. (1984). *J. Phys. E Sci. Instrum.* **17** (6): 521–525.
Imhof, R.E., McKendrick, A.D., and Xiao, P. (1995). *Rev. Sci. Instrum.* **66** (11): 5203–5213.
Ingle, J.D. Jr. and Crouch, S.R. (1988). *Spectrochemical Analysis*. Englewood Cliffs, NJ: Prentice Hall.
Jacinto, C., Messias, D.N., Andrade, A.A. et al. (2006). *J. Non Cryst. Solids* **352** (32–35): 3582–3597.
Jackson, W.B., Amer, N.M., Boccara, A.C., and Fournier, D. (1981). *Appl. Optics* **20**: 1333.
Jeon, R.J., Mandelis, A., and Abrams, S.H. (2003). *Rev. Sci. Instrum.* **74** (1): 380–383.
Karner, C., Mandel, A., and Träger, F. (1985). *Appl. Phys. A* **38**: 19.
Kenji, U., Akihide, H., Hiroko, K. et al. (2000). *Jpn. J. Appl. Phys.* **39** (9R): 5316.
Kerr, E.L. and Atwood, J.G. (1968). *Appl. Optics* **7**: 915.
Khodakovskaya, M.V., de Silva, K., Nedosekin, D.A. et al. (2011). *Proc. Natl. Acad. Sci. U. S. A.* **108** (3): 1028–1033.
Kim, S., Lee, D., Thundat, R. et al. (2012). *ESC Trans.* **50** (12): 459–464.
Kitamori, T. (1999). *Tanpakushitsu Kakusan Koso* **44** (10): 1527–1531.
Kitamori, T. (2001). *Fresenius J. Anal. Chem.* **371** (2): 89–90.
Kitamori, T. and Sawada, T. (1991). *Spectrochem. Acta Rev.* **14**: 275.
Kitamori, T., Tokeshi, M., Hibara, A., and Sato, K. (2004). *Anal. Chem.* **76** (3): 52A–60A.
Kovsh, D.I., Hagan, D.J., and Van Stryland, E.W. (1999). *Opt. Express* **4** (8): 315–327.
Kozich, V.P., Marcano, A., Hernandez, F.E., and Castillo, J.A. (1994). *Appl. Spectrosc.* **48** (12): 1506–1512.
Kreuzer, L.B. (1971). *J. Appl. Phys.* **42**: 2934.
Kreuzer, L.B., Kenyon, N.D., and Patel, C.K.N. (1972). *Science* **177**: 347.
Kuo, P.K. and Munidasa, M. (1990). *Appl. Opt.* **29**: 5326.
Lai, H.M. and Young, K. (1982). *J. Acoust. Soc. Am.* **76**: 2000.
Landau, L.D. and Lifshitz, E.M. (1959). *Fluid Mechanics*. Reading, MA: Addison-Wesley.
Leite, R.C.C., Moore, R.S., and Whinnery, J.R. (1964). *Appl. Phys. Lett.* **5**: 141.
Li, B.C. (1990). *J. Appl. Phys.* **68**: 482.
Li, B.C., Mandelis, A., and Kish, Z.Z. (2004). *J. Appl. Phys.* **95** (3): 1042–1049.
Li, B.C., Shaughnessy, D., Mandelis, A. et al. (2004a). *J. Appl. Phys.* **96** (1): 186–196.
Li, B.C., Shaughnessy, D., Mandelis, A. et al. (2004b). *J. Appl. Phys.* **95** (12): 7832–7840.
Li, B.C., Shaughnessy, D., and Mandelis, A. (2005a). *Rev. Sci. Instrum.* **76** (6).
Li, B.C., Shaughnessy, D., and Mandelis, A. (2005b). *J. Appl. Phys.* **97** (2).
Li, C., Zhang, D., Slipchenko, M.N., and Cheng, J.-X. (2017). *Anal. Chem.* **89** (9): 4863–4867.
Lima, S.M., Andrade, A.A., Catunda, T. et al. (2001a). *J. Non Cryst. Solids* **284** (1–3): 203–209.
Lima, S.M., Sampaio, J.A., Catunda, T. et al. (2001b). *J. Non Cryst. Solids* **284** (1–3): 274–281.
Liu, M. and Franko, M. (2012). Theoretical analysis for sensitivity enhancement in broad-band thermal lens microscope. In: *Frontiers of Manufacturing Science and Measuring Technology ii, Pts 1 and 2* (ed. W.P. Sung, J.C.M. Kao and R. Chen), 1480–1483.

Liu, M. and Franko, M. (2014a). *Int. J. Thermophys.* **35** (12): 2178–2186.
Liu, M. and Franko, M. (2014b). *Crit. Rev. Anal. Chem.* **44** (4): 328–353.
Liu, M. and Franko, M. (2016). *Int. J. Thermophys.* **37** (7): 67.
Liu, Y., Baddour, N., and Mandelis, A. (2003). *J. Appl. Phys.* **94** (9): 5543–5548.
Liu, M., Korte, D., and Franko, M. (2012). *J. Appl. Phys.* **111** (3): 033109.
Liu, M., Novak, U., Plazl, I., and Franko, M. (2014). *Int. J. Thermophys.* **35** (11): 2011–2022.
Long, G.R. and Bialkowski, S.E. (1985). *Anal. Chem.* **57**: 1079.
Long, M.E., Swofford, R.L., and Albrecht, A.C. (1976). *Science* **191**: 183.
Longaker, P.R. and Litvak, M.M. (1969). *J. Appl. Phys.* **40**: 4033.
Luk'yanov, A.Y. (2000). *Tech. Phys. Lett.* **26** (12): 1093–1095.
Luk'yanov, A.Y. and Novikov, M.A. (2000). *Tech. Phys.* **45** (11): 1470–1474.
Luk'yanov, A.Y. and Pogorelko, A.A. (2002). *Tech. Phys.* **47** (5): 585–590.
Luk'yanov, A.Y., Vladykin, G.B., Novikov, M.A., and Yashin, Y.I. (1999). *J. Anal. Chem. (Russ.)* **54** (7): 633–638.
Luk'yanov, A.Y., Bendrysheva, S.N., Proskurnin, M.A. et al. (2003). *Rev. Sci. Instrum.* **74** (1): 656–658.
Malacarne, L.C., Sato, F., Pedreira, P.R.B. et al. (2008). *Appl. Phys. Lett.* **92**: 131903.
Mandelis, A. (ed.) (1987). *Photoacoustic and Thermal Wave Phenomena in Semiconductors*. New York: North-Holland.
Mandelis, A. (2005). *J. Appl. Phys.* **97** (8).
Mandelis, A. and Tolev, J. (2008). *Eur. Phys. J. Special Topics* **153**: 387–390.
Mandelis, A. and Xia, J. (2008). *J. Appl. Phys.* **103** (4).
Mandelis, A., Batista, J., and Shaughnessy, D. (2003). *Phys. Rev. B* **67** (20).
Mandelis, A., Batista, J., Gibkes, J. et al. (2005a). *J. Appl. Phys.* **97** (8).
Mandelis, A., Batista, J., Pawlak, M. et al. (2005b). *J. Phys. IV* **125**: 565–567.
Mandelis, A., Pawlak, M., Wang, C.H. et al. (2005c). *J. Appl. Phys.* **98** (12).
Mawatari, K., Ohashi, T., Ebata, T. et al. (2011). *Lab Chip* **11** (17): 2990–2993.
Mawatari, K., Tsukahara, T., Tanaka, Y. et al. (2012). *Extended-nanofluidic Systems for Chemistry and Biotechnology, Extended-Nanofluidic Systems for Chemistry and Biotechnology*. London: Imperial College Press.
McDonald, F.A. (1986). *Can. J. Phys.* **64**: 1023.
McLean, E.A., Sica, L., and Glass, A. (1968). *J. Appl. Phys. Lett.* **13**: 369.
Meyer, P.L. and Sigrist, M.W. (1990). *Rev. Sci. Instrum.* **61**: 1779.
Mian, S.M., McGee, S.B., and Melikechi, N. (2002). *Opt. Comm.* **207** (1–6): 339–345.
Mori, K., Imashaka, T., and Ishibashi, N. (1982). *Anal. Chem.* **54**: 2034.
Morozov, A.I., Novikov, S.N., and Raevskii, V.Y. (1992). *Russ. J. Nondestr. Test.* **28** (1): 43–45.
Morris, M.D. and Fotiou, F.K. (1987). *Anal. Chem.* **59**: 185.
Morsch, S., Bastidas, P.D., and Rowland, S. (2017). *J. Mater. Chem. A* **5** (46): 24508–24517.
Murphy, J.C. and Aamodt, L.C. (1980). *J. Appl. Phys.* **51**: 4580.
Murphy, J.C. and Aamodt, L.C. (1981). *Appl. Phys. Lett.* **38**: 196.
Murphy, J.C., Maclachlan, J.W., and Aamodt, L.C. (1986). *IEEE Trans. Ultrason. Ferroelectr. Freq. Control* **UFFC-33**: 529.
Nedosekin, D.A., Shashkov, E.V., Galanzha, E.I. et al. (2010). *Cytometry A* **77A** (11): 1049–1058.
Nedosekin, D.A., Sarimollaoglu, M., Ye, J.H. et al. (2011). *Cytometry A* **79** (10): 825–833.
Nedosekin, D.A., Galanzha, E.I., Ayyadevara, S. et al. (2012a). *Biophys. J.* **102** (5): 1235–1235.
Nedosekin, D.A., Galanzha, E.I., Ayyadevara, S. et al. (2012b). *Biophys. J.* **102** (3): 672–681.
Nedosekin, D.A., Sarimollaoglu, M., Galanzha, E.I. et al. (2012c). *J. Biophotonics* **6**: 425–434.
Nedosekin, D.A., Juratli, M.A., Sarimollaoglu, M. et al. (2013). *J. Biophotonics* **6** (6–7): 523–533.
Nedosekin, D.A., Galanzha, E.I., Dervishi, E. et al. (2014). *Small* **10** (1): 135–142.
Nordal, P.-E. and Kanstad, S.O. (1979). *Phys. Scr.* **20**: 659.

Notingher, I. and Imhof, R.E. (2004). *Skin Res. Technol.* **10** (2): 113–121.
Notingher, I., Xiao, P., Imhof, R.E. et al. (2001). *Anal. Sci.* **17**: S486–S489.
Notingher, I., Imhof, R.E., Xiao, P., and Pascut, F.C. (2003). *Rev. Sci. Instrum.* **74** (1): 346–348.
Nyquist, R.A., Leugers, M.A., McKelvy, M.L. et al. (1990). *Anal. Chem.* **62**: 223R.
Olivares, J.A., Garcia-Valenzuela, A., Cuppo, F.L.S. et al. (2005). *J. Phys. IV* **125**: 153–156.
Olmstead, M.A., Amer, N.M., Kohn, S. et al. (1983). *Appl. Phys. A* **32**: 141.
Pao, Y.-H. (ed.) (1977). *Opto-acoustic Spectroscopy and Detection*. New York: Academic Press.
Papernov, S., Tait, A., Bittle, W. et al. (2011). *J. Appl. Phys.* **109** (11): 113106.
Parker, J.G. (1973). *Appl. Optics* **12**: 2974.
Patel, C.K.N. and Tam, A.C. (1981). *Rev. Mod. Phys.* **53**: 517.
Patel, C.K.N., Kerl, R.J., and Burkhardt, E.G. (1977). *Phys. Rev. Lett.* **38**: 1204.
Pelletier, M.J. and Harris, J.M. (1983). *Anal. Chem.* **54**: 1537.
Pelletier, M.J., Thornsheim, H.R., and Harris, J.M. (1982). *Anal. Chem.* **54**: 239.
Pilla, V., Catunda, T., Balogh, D.T. et al. (2002a). *J Polym Sci B* **40** (17): 1949–1956.
Pilla, V., Mendonca, C.R., Balogh, D., and Zilio, S.C. (2002b). *Mol. Cryst. Liq. Cryst.* **374**: 487–492.
Pleitez, M.A., Hertzberg, O., Bauer, A. et al. (2015). *Analyst* **140** (2): 483–488.
Pollock, H.M. and Hammiche, A. (2001). *J. Phys. D Appl. Phys.* **34** (9): R23–R53.
Pollock, H.M., Hammiche, A., and Song, M. (1996). *Abstr. Pap. Am. Chem. Soc.* **212**: 246–POLY.
Price, D.M., Reading, M., Hammiche, A., and Pollock, H.M. (1999). *Int. J. Pharm.* **192** (1): 85–96.
Proskurnin, M.A. (2014). 11 - photothermal spectroscopy. In: *Laser Spectroscopy for Sensing* (ed. M. Baudelet), 313–361. Cambridge: Woodhead Publishing.
Proskurnin, M.A. and Kononets, M.Y. (2004). *Usp. Khim.* **73** (12): 1235–1268.
Proskurnin, M.A., Slyadnev, M.N., Tokeshi, M., and Kitamori, T. (2003). *Anal. Chim. Acta* **480** (1): 79–95.
Proskurnin, M.A., Zhidkova, T.V., Volkov, D.S. et al. (2011). *Cytometry A* **79A** (10): 834–847.
Proskurnin, M.A., Volkov, D.S., Gor'kova, T.A. et al. (2015). *J. Anal. Chem. (Russ.)* **70** (3): 249–276.
Proskurnin, M.A., Bendrysheva, S.N., and Smirnova, A.P. (2016). *J. Anal. Chem. (Russ.)* **71** (5): 431–458.
Putzig, C.L., Leugers, M.A., McKelvy, M.L. et al. (1990). *Anal. Chem.* **62**: 223R.
Radovanović, T., Liu, M., Likar, P. et al. (2015). *Int. J. Thermophys.* **36** (5): 932–939.
Raduenz, R., Rings, D., Kroy, K., and Cichos, F. (2009). *J. Phys. Chem. A* **113** (9): 1674–1677.
Ragozina, N., Heissler, S., Faubel, W., and Pyell, U. (2002). *Anal. Chem.* **74** (17): 4480–4487.
Ragozina, N.Y., Putz, M., Heissler, S. et al. (2004). *Anal. Chem.* **76** (13): 3804–3809.
Reading, M., Price, D.M., Grandy, D.B. et al. (2001). *Macromol. Symp.* **167**: 45–62.
Reading, M., Grandy, D., Hammiche, A. et al. (2002). *Vib. Spectrosc.* **29** (1–2): 257–260.
Rosencwaig, A. (1977). *Opto-acoustic Spectroscopy and Detection* (ed. Y.-H. Pao). New York: Academic Press.
Rosencwaig, A. (1980). *Photoacoustics and Photoacoustic Spectroscopy*. New York: Wiley.
Sato, F., Malacarne, L.C., Pedreira, P.R.B. et al. (2008). *J. Appl. Phys.* **104**: 053520.
Sell, J.A. (ed.) (1989). *Photothermal Investigations in Solids and Fluids*. New York: Academic Press.
Selmke, M., Braun, M., and Cichos, F. (2012a). *J. Opt. Soc. Am. A* **29** (10): 2237–2241.
Selmke, M., Braun, M., and Cichos, F. (2012b). *ACS Nano* **6** (3): 2741–2749.
Selmke, M., Schachoff, R., Braun, M., and Cichos, F. (2013). *RSC Adv.* **3** (2): 394–400.
Sepaniak, M.J. and Kettler, C.N. (1984). *Abstr. Pap. Am. Chem. Soc.* **188** (AUG): 46-ANYL.
Shaughnessy, D. and Mandelis, A. (2006). *J. Electrochem. Soc.* **153** (4): G283–G290.
Shaughnessy, D., Li, B., Mandelis, A. et al. (2005). *J. Phys. IV* **125**: 447–449.
Shaughnessy, D., Mandelis, A., and Batista, J. (2005). *J. Phys. IV* **125**: 561–563.
Shaughnessy, D., Mandelis, A., Batista, J. et al. (2006). *Semicond. Sci. Technol.* **21** (3): 320–334.
Sheik-Bahae, M., Said, A.A., Wei, T.-H. et al. (1990). *IEEE J. Quantum Electron.* **24** (4): 760–769.

Shimizu, H., Mawatari, K., and Kitamori, T. (2011). *J. Sep. Sci.* **34** (20): 2920–2924.
Siebert, D.R., Grabiner, F.R., and Flynn, G.W. (1974). *J. Chem. Phys.* **60**: 1564.
Sinha, S., Ray, A., and Dasgupta, K. (2000). *J. Appl. Phys.* **87** (7): 3222–3226.
Slatkine, M. (1981). *Appl. Optics* **20**: 2880.
Smirnova, A., Proskurnin, M.A., Mawatari, K., and Kitamori, T. (2012). *Electrophoresis* **33** (17): 2748–2751.
Snook, R. (1997). *Chem. Soc. Rev.* **26** (4): 319–326.
Solomini, D. (1966). *J. Appl. Phys.* **12**: 3314.
Stephenson, J.C., Wood, R.E., and Moore, C.B. (1968). *J. Chem. Phys.* **48**: 4790.
Stone, J.J. (1972). *Opt. Soc. Am.* **62**: 327.
Stone, J. (1973). *Appl. Optics* **12**: 1828.
Swofford, R.L. and Morrell, J.A. (1978). *J. Appl. Phys.* **49**: 3667.
Tam, A.C. (1983). *Ultrasensitive Laser Spectroscopy* (ed. D.S. Kliger). New York: Academic Press.
Tam, A.C. (1985). *Infrared Phys.* **25**: 305.
Tam, A.C. (1986). *Rev. Mod. Phys.* **58**: 381.
Tam, A.C. (1989). *Photothermal Investigations in Solids and Fluids* (ed. J.A. Sell). New York: Academic Press.
Tam, A.C. and Sullivan, B. (1983). *Appl. Phys. Lett.* **43** (4): 333–335.
Terazima, M. (1995). *Opt. Lett.* **20** (1): 25–27.
Tokeshi, M., Minagawa, T., and Kitamori, T. (2000). *Anal. Chem.* **72** (7): 1711–1714.
Tokeshi, M., Uchida, M., Hibara, A. et al. (2001). *Anal. Chem.* **73**: 2112.
Tuchin, V.V., Tárnok, A., and Zharov, V.P. (2011). *Cytometry A* **79A** (10): 737–745.
Twarowski, A.J. and Kliger, D.S. (1977a). *Chem. Phys.* **20**: 253.
Twarowski, A.J. and Kliger, D.S. (1977b). *Chem. Phys.* **20**: 259.
Viengerov, M.L. (1938). *Dokl. Akad. Nauk SSSR* **19**: 687.
Weimer, W.A. and Dovichi, N.J. (1988). *Anal. Chem.* **60**: 662.
Weston, A. and Brown, P.R. (1997). *High Performance Liquid Chromatography & Capillary Electrophoresis: Principles and Practices*. Elsevier Science.
Whinnery, J.R. (1974). *Acc. Chem. Res.* **7**: 225.
Xiao, P. (2016). *Cosmetics* **3** (1): 10.
Xiao, P., Cowen, J.A., and Imhof, R.E. (2001). *Anal. Sci.* **17**: S349–S352.
Xiao, P., Cowen, J.A., and Imhof, R.E. (2003). *Rev. Sci. Instrum.* **74** (1): 767–769.
Yamamoto, T., Kazoe, Y., Mawatari, K., and Kitamori, T. (2011). *J. Synth. Org. Chem. Jpn.* **69** (5): 526–533.
Yardley, J.T. and Moore, C.B. (1966). *J. Chem. Phys.* **45**: 1066.
Zhang, D., Li, C., Zhang, C. et al. (2016). *Sci. Adv.* **2** (9).
Zharov, V.P. (1986). *Laser Opto-acoustic Spectroscopy in Chromatography in Laser Analytical Spectrochemistry* (ed. V.S. Letokhov). Boston, MA: Adam Hilger.
Zharov, V.P. and Letokhov, V.S. (1986). *Laser Optoacoustic Spectroscopy*. New York: Springer-Verlag.
Zharov, V., Waner, M., Lapotko, D., and Romanovskaya, T. (2002). *Lasers Surg. Med.* **30** (S14): 86–86.
Zhu, X.R., McGraw, D.J., and Harris, J.M. (1992). *Anal. Chem.* **64**: 710A.